

**Effect of Hull-to-Bulkhead Flexible Connection on
Blast Resistance of Double Hulled Ships**

by

Christian R. Brown

B.Eng., Mechanical Engineering
Royal Military College of Canada, 1997

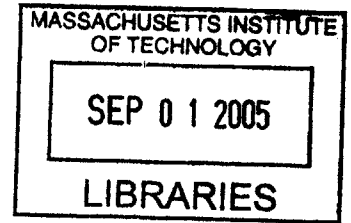
Submitted to the Department of Ocean Engineering
and the Department of Mechanical Engineering in
Partial Fulfillment of the Requirements of the Degrees of

Master of Naval Architecture and Marine Engineering

and

Master of Science in Mechanical Engineering


at the
Massachusetts Institute of Technology
June 2004

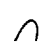


© 2004 Massachusetts Institute of Technology
All Rights Reserved

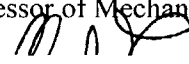
Signature of Author

Department of Ocean Engineering
May 7, 2004


Certified by 


Tomasz Wierzbicki
Professor of Applied Mechanics
Thesis Supervisor

Certified by


Simona Socrate
Professor of Mechanical Engineering
Thesis Reader

Accepted by


Michael S. Triantafyllou
Professor of Ocean Engineering
Chair, Departmental Committee on Graduate Studies

Accepted by


Ain A. Sonin
Professor of Mechanical Engineering
Chair, Departmental Committee on Graduate Studies

BARKER

Handwritten notes or a small diagram, possibly related to a list or table, located in the upper left quadrant of the page. The text is very faint and illegible.

Handwritten notes or a small diagram, possibly related to a list or table, located in the lower left quadrant of the page. The text is very faint and illegible.

Effect of Hull-to-Bulkhead Flexible Connection on Blast Resistance of Double Hulled Ships

by

Christian R. Brown

Submitted to the Department of Ocean Engineering and the
Department of Mechanical Engineering on May 7, 2004 in
Partial Fulfillment of the Requirements of the Degrees of
Master of Naval Architecture and Marine Engineering and
Master of Science in Mechanical Engineering

ABSTRACT

The use of double hull construction is commonplace within the shipping industry though it is largely unexploited within naval vessels. The Impact and Crashworthiness Lab at MIT has proposed the use of adaptive sandwich structures to improve the blast resistance of naval hulls. This project will address two main areas of investigation through the use of simplified analytical models: the integration of hardening and softening plastic core responses in the crushing of a rigidly supported sandwich panel; and the deformation analysis of a sandwich panel supported by non-rigid connections. The analytical solutions were utilized to perform a series of parametric studies to evaluate both the useable range of the models as well as to investigate the general behavior of a sandwich panel under a uniform load when supported by crushable connections. This initial investigation provides the simplified tools to begin and to validate a more detailed, numerical analysis.

Thesis Supervisor: Tomasz Wierzbicki
Title: Professor of Applied Mechanics

Table of Contents

ABSTRACT.....	3
ACKNOWLEDGEMENTS.....	7
LIST OF FIGURES	9
LIST OF TABLES.....	13
INTRODUCTION	15
1.1 Overview.....	15
1.2 Motivation.....	16
CRUSH RESPONSE OF A SANDWICH PANEL.....	18
2.1 Introduction.....	18
2.2 Formulation of the Problem and General Solution.....	20
2.3 Solution for a Hardening/Softening Core Model.....	22
2.4 Solution for a Hardening/Softening Model with a Rectangular Punch.....	24
2.5 Comparison of Hardening Softening and Limiting Core Responses.....	28
2.6 Parametric Analysis of Crush Response Models.....	31
2.7 Equation Summary.....	33
CRUSH RESPONSE OF SUPPORTS.....	35
3.1 Introduction.....	35
3.2 Analytical Solutions for Simple Cross-Sections.....	35
MODELLING OF SUPPORTED SANDWICH PANEL.....	40
4.1 Introduction.....	40
4.2 Standard Beam Bending Model.....	40
4.3 Plate Bending Model With Crushable Connections.....	45
4.4 Analysis of Quasi-Static Load Response.....	53
4.5 Numerical Example.....	60
4.6 Summary of Relevance to Hull Failure.....	61
CONCLUSIONS AND RECOMMENDATIONS.....	63
5.1 Conclusions.....	63
5.2 Recommendations.....	64
BIBLIOGRAPHY.....	65

Acknowledgements

First, I want to thank Professor Tomasz Wierzbicki for his patience and persistence in spite of me. His guidance and direction were absolutely instrumental in my successful completion of this thesis. I would also like to thank Professor Simona Socrate for her graciousness; I am truly thankful for her last minute support.

More importantly, I have to thank my fiancée, Leann Arseneau. She gave up a lot by leaving her family, friends and Country to travel across the continent with me into an uncertain future. Lee has supported me, been my best friend, my only fan and most recently the single driving and encouraging force behind my achievements. These past two years were about me and for me; I can only hope that pledging the rest of my life to her will allow me the opportunity to return the favor of her commitment and sacrifice.

List of Figures

Figure 1 – Damaging of the USS Cole.	15
Figure 2 – Sandwich Core Configurations.....	16
Figure 3 – Proposed Sandwich Panel Attachment Displaying Crushable Connection.....	16
Figure 4 – Definition of a Ship’s Hull Section.	17
Figure 5 – Geometry of Rigidly Supported Sandwich Panel Subject to a Knife Edge Punch Indentation.	18
Figure 6 – Geometry of Rigidly Supported Sandwich Panel Subject to a Rectangular Punch Indentation.	19
Figure 7 – Assumed Limiting, Hardening and Softening Responses for Sandwich Core.	19
Figure 8 – Unit Element of Deformed Face Plate.....	20
Figure 9 – Geometry of Rigidly Supported Sandwich Panel Subject to a Rectangular Punch Indentation.	25
Figure 10 – Boundary Condition Based on Force Balance at $x = r$	26
Figure 11 – Comparison of Maximum Deflections for Knife Edge Loading.....	28
Figure 12 – Comparison of the Normalized Force for Knife Edge Loading.	29
Figure 13 – Comparison of Maximum Deflection for Rectangular Punch Loading.	30
Figure 14 – Comparison of Normalized Force for Rectangular Punch Loading.....	31
Figure 15 – Parametric Analysis of Varying E_t/σ_0 for Hardening Core Response.....	32
Figure 16 – Parametric Analysis of Varying E_t/σ_0 for Softening Core Response.	32
Figure 17 – Proposed Sandwich Panel Attachment Displaying Crushable Connection.....	35
Figure 18 – Idealized Cross-Sections from Wierzbicki and Abramowicz [5].....	36
Figure 19 – Load-Displacement Characteristics of Rings with Stationary and Moving Hinges. From Wierzbicki and Abramowicz [3]	37
Figure 20 – Numerical Load-Displacement Versus Analytical Solution (Dashed Line) for Crushing of a Ring with Moving Hinges. From Wierzbicki and Abramowicz [5]	37

Figure 21 – Crushing of an Un-braced Diamond Cross Section.	38
Figure 22 – Load-Displacement Curve for an Un-braced Diamond Cross-Section.	38
Figure 23 – Beam Bending Model.	41
Figure 24 – Description of Modeled Square Honeycomb Core. From Xue and Hutchinson [6].	43
Figure 25 – Stress-Strain Representation of Honeycomb Core. From Xue and Hutchinson [6].	43
Figure 26 – Comparison of Load Displacement Curves.	45
Figure 27 – Theoretical Set-up for a Sandwich Plate on Crushable Supports.	46
Figure 28 – Assumed Plastic Hinge-Line Deformation.	46
Figure 29 – Assumed Shear Response and Related Shear Zones of Core.	50
Figure 30 – Assumed Softening Response and Equation for Crushable Connections.	51
Figure 31 – Crushable Connection Load-Displacement Functions.	54
Figure 32 – Load-Displacement for Hardening Crushable Connections, Case 1.	55
Figure 33 – Load-Displacement for Hardening Crushable Connections, Case 2.	55
Figure 34 – Load-Displacement for Softening Crushable Connections, Case1.	56
Figure 35 – Load-Displacement for Softening Crushable Connections, Case 2.	57
Figure 36 – Load-Displacement for Circular Section Crushing, Case 1.	57
Figure 37 – Load-Displacement for Circular Section Crushing, Case 2.	58
Figure 38 – Load-Displacement for Diamond Section Crushing, Case 1.	59
Figure 39 – Load-Displacement for Diamond Section Crushing, Case 2.	59
Figure 40 – Parametric Analysis of Varying Ratio of Initial Rigidity of Crushable Connections to Initial Rigidity of Sandwich Panel	61
Figure 41 – Energy Dissipation for a Rigidly Supported Sandwich Panel.	62
Figure 42 – Combined Energy Dissipation for a Sandwich Panel on Crushable Support.	62

List of Tables

Table 1 – Summary of Equations for Sandwich Plate Crushing 33

Chapter 1

INTRODUCTION

1.1 Overview

The use of large double hulls is soon to be law within the oil transport industry. The implementation of a double-hull configuration is intended to increase a tankers ability to remain intact after an accidental loading such as a collision or grounding. Although the use of a double-hull is wide spread in civilian ships, the benefits remain largely untapped in the Navy. The damaging of the USS Cole (figure 1) was a sobering example of the new threat that naval forces face. Naval vessels have traditionally relied upon compartmentalization and rapid response to avert sinking and minimize the damage due to blasts. Although, this arrangement provides for a robust level of survivability, it does not provide any protection to personnel or equipment in the vicinity of the blast, nor does it allow for the absorption of higher energy incidents that may jeopardize the ship's overall structural integrity.

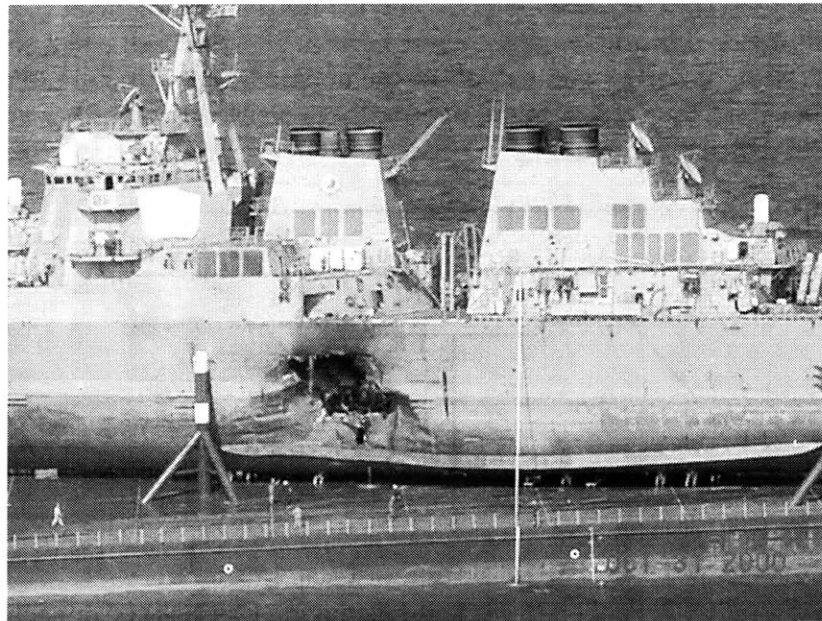


Figure 1 – Damaging of the USS Cole.

The Impact and Crashworthiness Lab has extended its work in automotive crash resistance to the investigation of the effect of adaptive cores within a sandwich plate construction that may re-distribute and/or absorb increased energy and reduce the incidence of punch through in the presence of a proximity blast.

An adaptive core structure has been numerically modeled and has initially demonstrated increased fracture resistance when compared to a single plate as well as when compared to a unidirectionally stiffened panel, see figure 2. These results indicate the

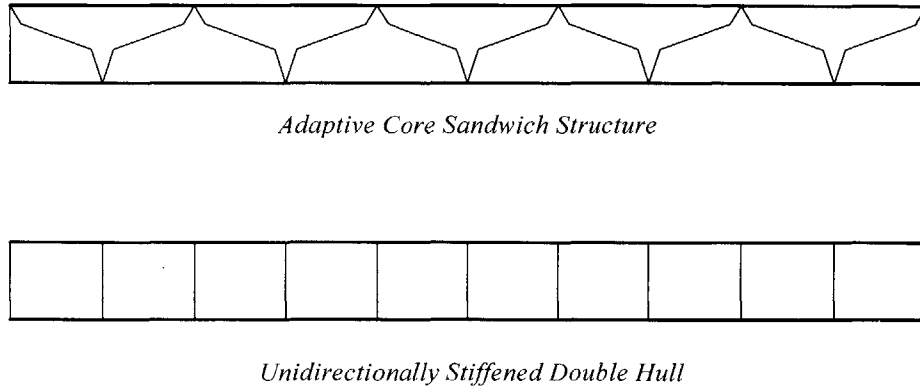


Figure 2 – Sandwich Core Configurations.

potential benefit of using an adaptive core hull structure. The current numerical model is arranged in a clamped-clamped configuration simulating the plate’s attachment to the rigid upper and lower decks and the two rigid transverse bulkheads. This arrangement necessarily limits the deformation to a single watertight section with the two rigid transverse bulkheads acting as stress risers. In order for a ship’s hull to further benefit from the adaptive core structure it is proposed that the blast energy may be spread out over adjacent sections through the use of a crushable interface between the hull and the transverse bulkhead as shown in the following figure, figure 3. The implementation of a crushable stool will add a secondary means for the absorption of energy and will allow the double hulled structure to potentially deform over greater spans, thus reducing the possibility of fracture and further increasing the overall level of blast damage survivability

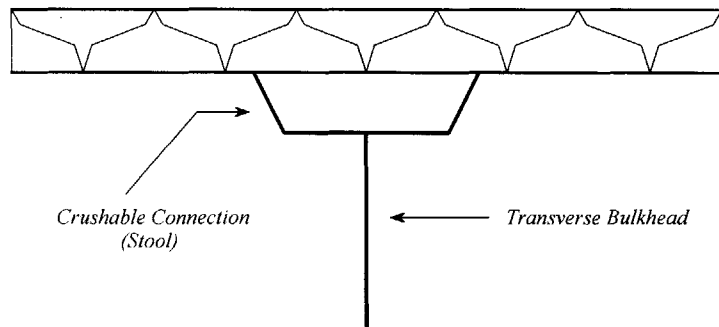


Figure 3 – Proposed Sandwich Panel Attachment Displaying Crushable Connection.

1.2 Motivation

It is the goal of this thesis to describe, through the use of simplifying assumptions and an analytical model, the deformation associated with a sandwich panel supported by a crushable stool under quasi-static loading. More specifically, what will be modeled is a single ship’s section, which will be defined as extending between two main transverse

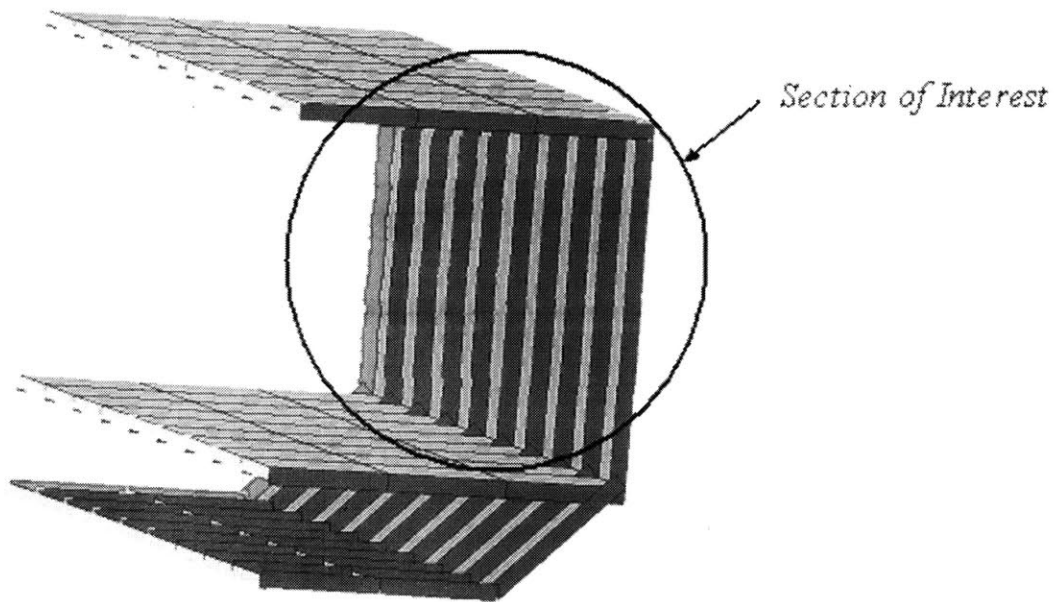


Figure 4 – Definition of a Ship's Hull Section.

bulkheads and two main decks as indicated in figure 4. This section essentially makes up a single panel, supported around its periphery by the decks and the main transverse bulkheads. However, it is at these points of connection for which it is proposed that a crushable support be included between the hull panel and the surrounding decks and transverse bulkheads. The analytical analysis for such a problem can span from a very simple beam approximation to a higher order three dimensional interpretation with core crushing. The aim of this thesis is to investigate the phenomenon without excessive complication to obtain an understanding of the first order behavior of a sandwich panel on crushable supports. The analysis of the crushing of a rigidly supported sandwich panel will be derived in closed form for a quasi-static indentation using both a knife edged punch and a rectangular punch. The solution will utilize a kinematic boundary condition to model the moving zone of plastic deformation with respect to which the total resisting force will then be minimized, similar to an analysis carried out by Wierzbicki and Suh [1]. This analysis will be repeated for both softening and hardening responses of the core followed by a parametric analysis of the deformation associated with differing core properties. The analysis of the sandwich panel will follow through successive levels of complexity making use of standard variational/energy methods and plastic yield-line deformation mechanisms.

The main goal of this research was to produce the initial characterization and quantification of the response of a sandwich panel; therefore, no consideration was given to the practical implementation of the results found herein. That is, the design and manufacturing requirements for a sandwich panel along with the associated weight implications were not addressed. Furthermore, the geometric design of the crushable stool and its proper integration with the sandwich panel was left for further study with the support of numerical tools.

Chapter 2

CRUSH RESPONSE OF A SANDWICH PANEL

2.1 Introduction

The initial background work of this project involved the production of an analytical description of the crushing of general sandwich panel on a rigid base. The panel was described as consisting of a face sheet of thickness h on top of a crushable core of thickness H . This general configuration was then mathematically exposed to two different force applications. The first load was a knife edge punch indentation as shown in figure 5. This point load can be seen to represent a collision or grounding loading of a ship's hull.

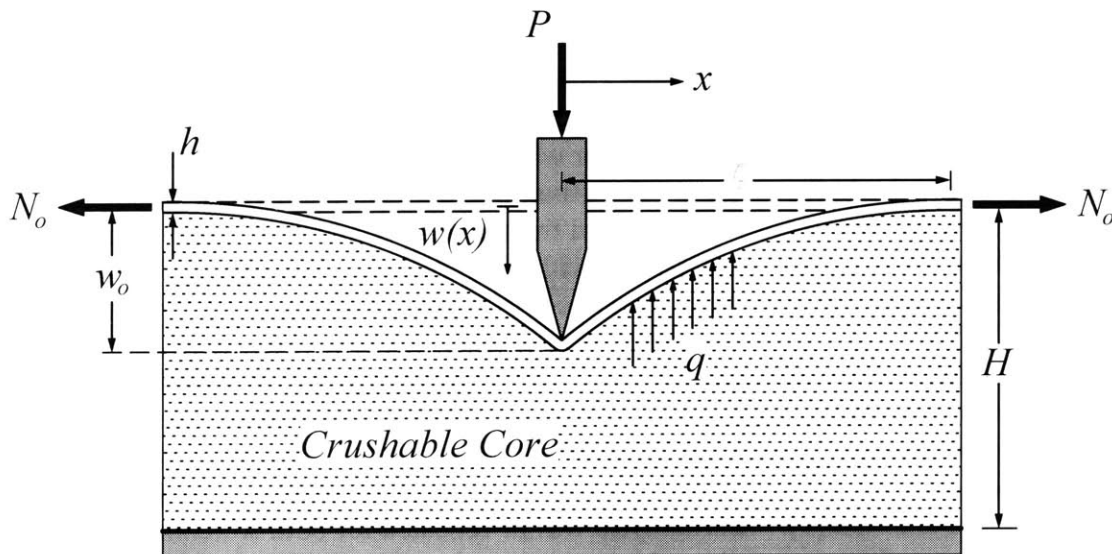


Figure 5 – Geometry of Rigidly Supported Sandwich Panel Subject to a Knife Edge Punch Indentation.

The nomenclature displayed within Figure 5 includes the location of a moving plastic hinge ζ , the sandwich core's crushing load q , the membrane force N_o within the face plate and the maximum displacement of the face plate w_0 . This nomenclature was retained throughout this thesis, while this model formed the initial basis from which the subsequent, more complicated models were derived.

Altering the application of the load from a knife edge to a flat or rectangular punch helped to create a scenario which could be seen as more closely resembling a localized blast

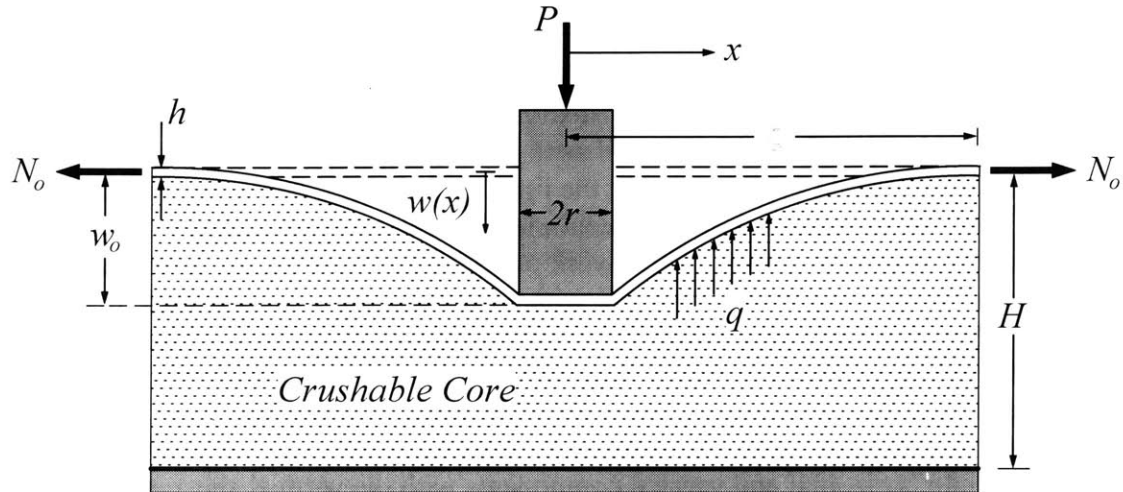


Figure 6 – Geometry of Rigidly Supported Sandwich Panel Subject to a Rectangular Punch Indentation.

loading. The assumed configuration for the flat punch model is shown in figure 6 where the notation remains the same as was previously described for the knife edge punch. In order to evaluate various characteristics of this model, different attributes were give to the core's material, that is, q was treated as a function of the shear strain produced by the deformation of the face plate. The response function of the core was thus varied through three different constitutive models as shown in figure 7. The rigid-perfectly plastic response was chosen,

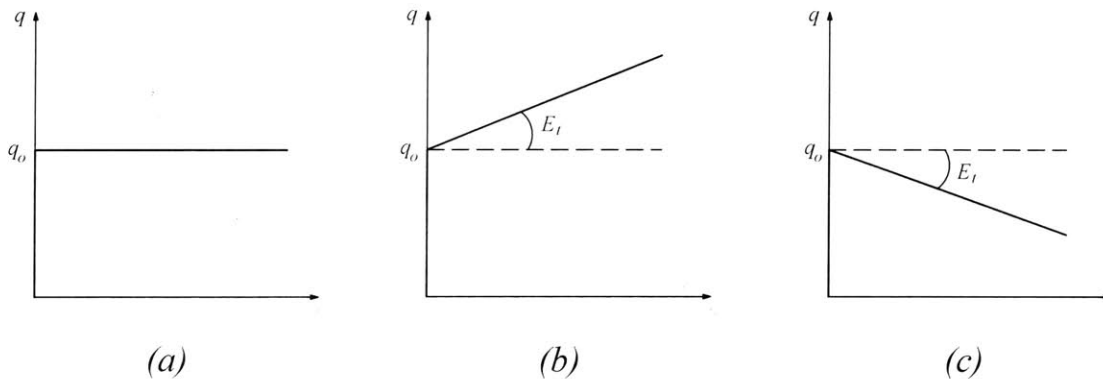


Figure 7 – Assumed Limiting, Hardening and Softening Responses for Sandwich Core.

due to its simplicity, as the initial limiting case. In order to gain more advanced insight into the problem of the crushing of a sandwich plate linear hardening and softening responses were also analyzed.

The following section describes the formulation of the general problem for the knife edge punch loading versus the limiting response. The work then expands to include the more complicated hardening and softening functions as well as introducing the added complication of a rectangular, flat faced punch.

2.2 Formulation of the Problem and General Solution

As initially described, the evaluation of the crush response of a sandwich panel was developed through increasing levels of complexity to provide insight into the behavior of the mathematics of an analytical solution as well as to provide a sound base upon which more complicated solutions could be compared in the limit. Wierzbicki, de Lacruz Alvarez and Hoo Fatt [2] describe the essential development of an indentation with radial symmetry utilizing a moving plastic boundary. Their work provided the basis for the formulation of this plane stress background study. To begin with a limiting case was examined; it is described in figure 5: a knife edge punch indentation using a rigid-perfectly plastic core response relationship, as shown in figure 7(a), for the behavior of the sandwich material.

To determine the governing equation for the deflection of the face plate under a knife edge loading a unit element, as shown in figure 8, was examined. The membrane force, N_o , is decomposed into horizontal and vertical components with the vertical shear component labeled Q and the local slope of the face plate, designated as α . The resisting force per unit length q arises from the crushing of the sandwich core whose behavior is defined according to figure 7(a).

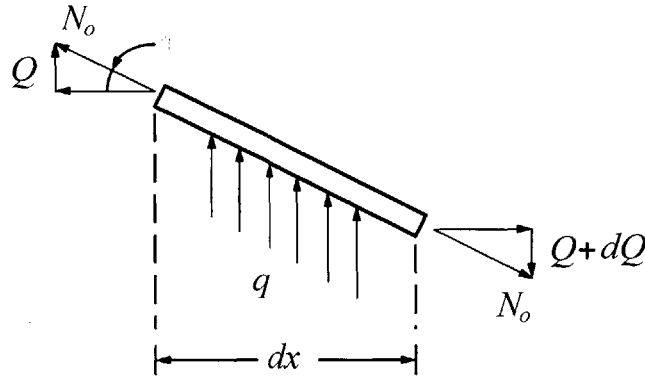


Figure 8 – Unit Element of Deformed Face Plate.

From a vertical force balance of a plate strip a relationship between the shear Q and the core crush resistance q can be found as

$$\frac{dQ}{dx} = q \quad (2.2.1)$$

For smaller deformations the slope of the face plate w' and the relationship between Q and N_o can be approximated as

$$\frac{dw}{dx} = \alpha \quad \text{and} \quad Q \approx N_o \cdot \alpha \quad (2.2.2)$$

By combining these equations and substituting into equation (2.2.1) the following governing equation is defined

$$\frac{d}{dx} \left(N_o \cdot \frac{dw}{dx} \right) = q \quad (2.2.3)$$

The fully plastic membrane force N_o will be constant with respect to x ; therefore, the general governing equation becomes

$$N_o \cdot w'' = q \quad (2.2.4)$$

where the double prime denotes differentiation with respect to the coordinate x -axis. This differential equation can now be solved utilizing the relationship in figure 7(a) for q . Since q is constant in this limiting case we can simplify equation (2.2.4) by defining

$$\bar{q} \equiv \frac{q_o}{N_o} \quad (2.2.5)$$

to yield the final governing equation for the limiting case

$$w'' = \bar{q} \quad (2.2.6)$$

The second order governing equation will be subject to two boundary conditions: the displacement of the panel w at the edge of the plastic region ζ as shown in Figure 7 must be zero; and the total shear force developed in the face plate must equilibrate the difference between the indentation force P and the crush resistance of the core q . The knife edge loading produces a point load at $x = 0$ which is initially resisted only by the vertical component of the membrane force N_o . Thus, the governing equation is subject to the following boundary conditions

$$w = 0 \quad \text{at} \quad x = \zeta \quad (2.2.7)$$

and

$$w' = \frac{-P}{2 \cdot N_o} \quad \text{at} \quad x = 0 \quad (2.2.8)$$

By integrating equation (2.2.6) twice and utilizing the above boundary conditions the deformation of the panel w is described by equation (2.2.9) where the subscript L denotes the limiting condition:

$$w_L = \frac{1}{2} \cdot \left[\bar{q} \cdot x^2 - \frac{P}{N_o} \cdot x + \zeta \cdot \left(\frac{P}{N_o} - \bar{q} \cdot \zeta \right) \right] \quad (2.2.9)$$

Within equation (2.2.9) the boundary of plastic deformation ζ is a function of the load P and varies throughout the loading process. In order to reduce the variables in equation (2.2.9), Wierzbicki and Suh [1] showed that a relationship between P and ζ can be derived by minimizing the resisting force with respect to ζ . The minimization is carried out at $x=0$ such that $w(0)=w_o$ and removing dependence on x . Substituting $x=0$ into equation (2.2.9), noting that $w(0)=w_o$ and rearranging to solve for $P(\zeta)$:

$$P_L = \frac{2 \cdot w_o \cdot N_o}{\zeta} + N_o \cdot \bar{q} \cdot \zeta \quad (2.2.10)$$

Through the minimization of P with respect to ζ a relationship between the maximum deflection w_o and the extent of plastic deformation ζ is found to be:

$$w_{L,o} = \frac{1}{2} \cdot \bar{q} \cdot \zeta^2 \quad (2.2.11)$$

This solution for w_o can be used in equation (2.2.10) to find a force-boundary (P - ζ) equation for a sandwich panel subject to a knife edge loading:

$$P_l = 2 \cdot N_o \cdot \bar{q} \cdot \zeta \quad (2.2.12)$$

This solution for a minimized force-boundary equation can be used to simplify equation (2.2.9), the deflection profile, to:

$$w_l = \frac{1}{2} \cdot \bar{q} (x - \zeta)^2 \quad (2.2.13)$$

and normalizing by the equation for maximum deflection w_o the limiting normalized deflection profile for a point loading with a constant core reaction becomes:

$$w_l^{norm} = \frac{(x - \zeta)^2}{\zeta^2} \quad (2.2.14)$$

2.3 Solution for a Hardening/Softening Core Model

After the initial limiting case was solved, hardening and softening characteristics of the core were added to the mathematical model. The same force application geometry was used as in figure 7 however the assumed sandwich core reaction force q was refined to include either a hardening or a softening response during plastic deformation as shown in figure 7(b) and (c) respectively. In order to make use of these reactions an engineering strain ε will be defined as the ratio of the displacement of the face plate, which varies with x , to the thickness of the core H :

$$\varepsilon = \frac{w}{H} \quad (2.3.1)$$

Therefore, the sandwich core's reaction force q will be approximated using equation (2.3.1) as

$$q = q_o \pm E_t \cdot \varepsilon = q_o \pm \frac{E_t}{H} \cdot w \quad (2.3.2)$$

Substituting the assumed hardening and softening responses into equation (2.2.4), using the definition for \bar{q} in equation (2.2.5) and defining

$$k^2 \equiv \frac{E_t}{N_o H} \quad (2.3.3)$$

the governing equation for a knife edge punch indentation with a hardening and softening core responses becomes, respectively,

$$w'' - k^2 \cdot w = \bar{q} \quad \text{and} \quad w'' + k^2 \cdot w = \bar{q} \quad (2.3.4)$$

The governing equations are subject to the same boundary conditions as in the initial limiting case developed in Section 2.2, that is

$$w = 0 \quad \text{at} \quad x = \zeta \quad (2.3.5)$$

and

$$w' = \frac{-P}{2 \cdot N_o} \quad \text{at} \quad x = 0 \quad (2.3.6)$$

Solving the governing differential equation for a knife edge indentation with hardening yields an exponential solution for the deflection profile w_H , where the subscript H denotes a hardening core response:

$$w_H = C_1 e^{k \cdot x} + C_2 e^{-k \cdot x} - \frac{\bar{q}}{k^2} \quad (2.3.7)$$

and where,

$$C_1 = \frac{2N_o \bar{q} \cdot e^{k \cdot \zeta} - Pk}{2N_o k^2 (1 + e^{2k \cdot \zeta})} \quad \text{and} \quad C_2 = \frac{(2N_o \bar{q} \cdot e^{-k \cdot \zeta} + Pk) e^{2k \cdot \zeta}}{2N_o k^2 (1 + e^{2k \cdot \zeta})}$$

Once again to ensure that the kinematic condition that exists at the boundary ζ is maintained the load P at $x=0$ where $w=w_o$ is minimized with respect to ζ to arrive at a relationship between the maximum deflection w_o and the moving plastic boundary ζ . For the hardening case it can be shown that after minimization

$$w_{Ho} = \frac{\bar{q} (e^{k \cdot \zeta} - 1)^2}{2k^2 \cdot e^{k \cdot \zeta}} \quad (2.3.8)$$

Equating equation (2.3.8) to equation (2.3.7) evaluated at $x=0$ a compact expression for the load P as a function of the boundary ζ is found to be

$$P_H = \frac{\bar{q} \cdot N_o}{k} \cdot e^{k \cdot \zeta} (1 - e^{-2k \cdot \zeta}) \quad (2.3.9)$$

Furthermore, when taken in the limit as $E_i \rightarrow 0$ ($k \rightarrow 0$) equation (2.3.9) becomes equivalent to the load-boundary relationship, equation (2.2.12), for the limiting case.

Although the load and maximum deflection are important factors, the deformation function w_H also provides insight into the nature of the mathematics. The deformation as solved for in equation (2.3.7) is a function of x , P and ζ , to reduce this number of variables equation (2.3.9) can be utilized to produce a succinct equation in x and ζ

$$w_H = \frac{\bar{q} \cdot e^{k(x-\zeta)}}{2k^2} (e^{-k(x-\zeta)} - 1)^2 \quad (2.3.10)$$

Normalizing equation (2.3.10) by the maximum deflection w_o , solved for in (2.3.8), further simplifies the deformation function to

$$w_H^{norm} = e^{kx} \cdot \frac{(e^{k(\zeta-x)} - 1)^2}{(e^{k\zeta} - 1)^2} \quad (2.3.11)$$

To solve the governing differential equation for a knife edge indentation with softening an identical process is followed. The general solution, in complex exponentials,

was found to be

$$w_s = C_1 \cdot e^{i \cdot k \cdot x} + C_2 \cdot e^{-i \cdot k \cdot x} + \frac{\bar{q}}{k^2} \quad (2.3.12)$$

with the following constants determined from the boundary conditions in equation (2.3.5) and (2.3.6)

$$C_1 = \frac{-(2N_o \bar{q} \cdot e^{i \cdot k \cdot \zeta} - i \cdot Pk)}{2N_o k^2 (1 + e^{i \cdot 2k \cdot \zeta})} \quad \text{and} \quad C_2 = \frac{-(2N_o \bar{q} \cdot e^{-i \cdot k \cdot \zeta} + i \cdot Pk) \cdot e^{i \cdot 2k \cdot \zeta}}{2N_o k^2 (1 + e^{i \cdot 2k \cdot \zeta})}$$

The maximum deflection w_o as a function of the moving boundary ζ is then a cosine function

$$w_{s_o} = \frac{\bar{q}}{k^2} (1 - \cos(k \cdot \zeta)) \quad (2.3.13)$$

which, when equated to the differential solution evaluated at $x=0$, gives a simple expression for the load P as a function of the boundary ζ

$$P_s = \frac{2N_o \cdot \bar{q}}{k} \cdot \sin(k \cdot \zeta) \quad (2.3.14)$$

As with equation (2.3.9) when taken in the limit, equation (2.3.14) can also be shown to be equivalent to $P(\zeta)$ for the limiting case.

Substituting equation (2.3.14) into the solution for the deflection under a knife edge punch loading with a softening core response, equation (2.3.12), will reduce the number of variables to only x and ζ :

$$w_s = \frac{\bar{q}}{k^2} \{1 - \cos[k(x - \zeta)]\}. \quad (2.3.15)$$

As with the hardening response, this simplified equation can be further reduced by normalizing with respect to the maximum deflection w_o in equation (2.3.13) to produce

$$w_s^{norm} = \frac{\cos[k(x - \zeta)] - 1}{\cos(k\zeta) - 1} \quad (2.3.16)$$

By suitably non-dimensionalizing the above equations and utilizing some appropriate values, graphical comparisons of the hardening, softening and limiting reactions can be made.

2.4 Solution for a Hardening/Softening Model with a Rectangular Punch

The addition of a rectangular punch for the indentation of the panel will more closely reflect the geometry of the force from a close proximity blast. As shown in figure 6 and again here in figure 9 the rectangular punch is described by a width of $2r$. Making use of symmetry, the punch will be described as extending from $x=0$ to $x=r$ where the x -origin, quite naturally, is coincident with the centre of the punch. In order to mathematically evaluate the response of the sandwich panel under this type of loading, an identical process will be followed as was previously outlined for the knife edge punch. Moreover, the same assumed responses for the sandwich core material as illustrated in figure 7 will be used.

The initial governing differential equation remains the same as that determined in equation (2.2.4):

$$N_o \cdot w'' = q \quad (2.4.1)$$

and the sandwich core's assumed hardening and softening shear responses shown in figure 7 will be the same as for the knife edge punch in equation (2.3.2):

$$q = q_o \pm E_t \cdot \varepsilon = q_o \pm \frac{E_t}{H} \cdot w. \quad (2.4.2)$$

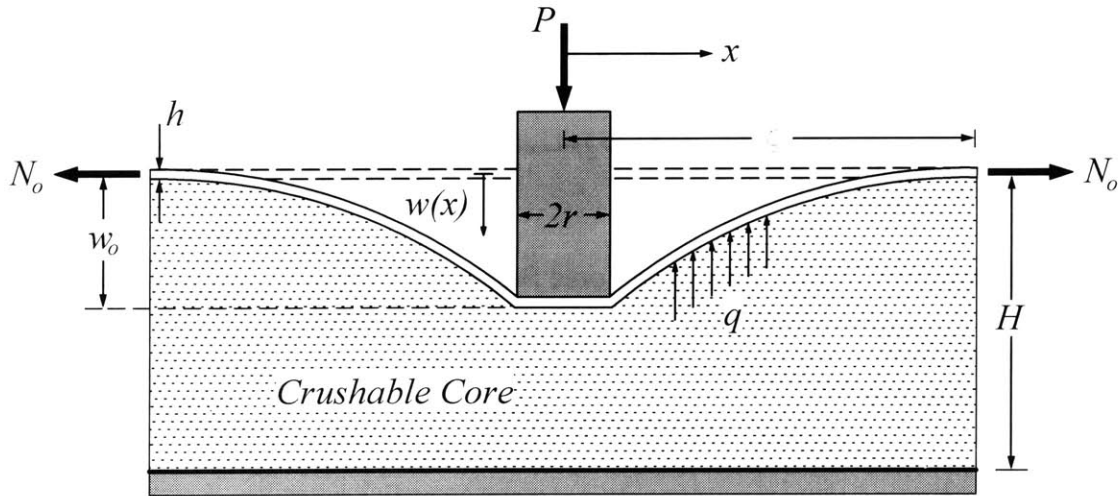


Figure 9 – Geometry of Rigidly Supported Sandwich Panel Subject to a Rectangular Punch Indentation.

Furthermore, combining of these equations will be simplified by defining \bar{q} and k^2 as before in equations (2.2.5) and (2.3.3) respectively. This will result in the specific governing equations for hardening and softening, respectively:

$$w'' - k^2 \cdot w = \bar{q} \quad \text{and} \quad w'' + k^2 \cdot w = \bar{q}. \quad (2.4.3)$$

These equations are identical to those shown for the knife edge indentation in equation (2.3.4). The integration of the punch is achieved through the boundary conditions specific to this problem. The displacement-plastic boundary condition remains the same:

$$w = 0 \quad \text{at} \quad x = \zeta; \quad (2.4.4)$$

however, the presence of the rectangular punch alters the force balancing boundary condition. With reference to figure 10 it can be shown, through a summation of the vertical forces and by making use of equations (2.2.2) and (2.4.2), that for a hardening core response the following relation exists from equilibrium:

$$2(N_o \cdot w') + P + 2r \cdot q_o + 2r \cdot \frac{E_t}{H} \cdot w = 0 \quad (2.4.5)$$

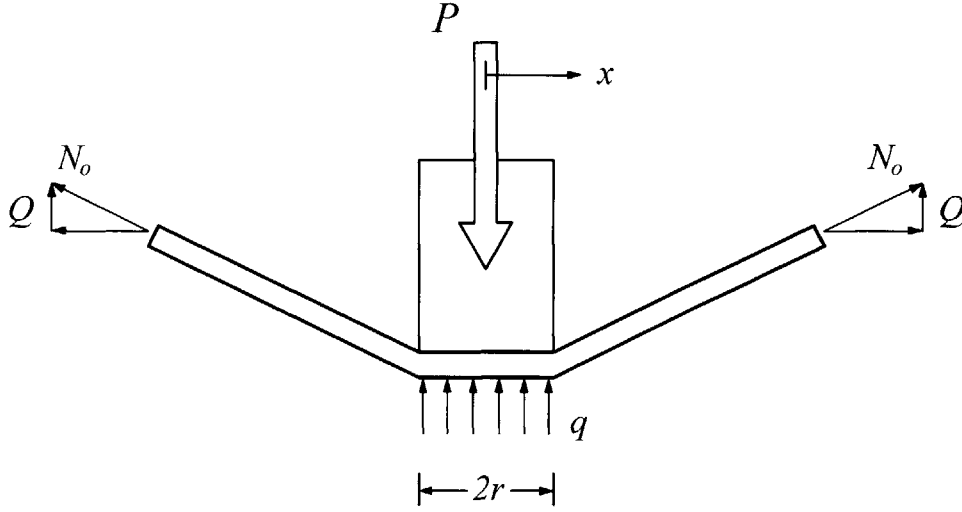


Figure 10 – Boundary Condition Based on Force Balance at $x = r$.

and for a softening core response:

$$2(N_o \cdot w') + P + 2r \cdot q_o - 2r \cdot \frac{E_t}{H} \cdot w = 0. \quad (2.4.6)$$

This boundary condition can be simplified by requiring it only at $x=r$ where $w=w_o$ and assuming that deformation from $x=0$ to $x=r$ is parallel to the face of the rectangular punch as illustrated in figure 10. Therefore, the second boundary condition for the hardening case becomes:

$$w' = - \left(\frac{P}{2N_o} + \bar{q} \cdot r + k^2 \cdot r \cdot w_o \right) \quad \text{at} \quad x = r, \quad (2.4.7)$$

while for the softening case, its second boundary condition becomes:

$$w' = - \left(\frac{P}{2N_o} + \bar{q} \cdot r - k^2 \cdot r \cdot w_o \right) \quad \text{at} \quad x = r \quad (2.4.8)$$

The general solution for the rectangular punch indentation with hardening will take the form:

$$w_H = C_1 e^{kx} + C_2 e^{-kx} - \frac{\bar{q}}{k^2} \quad (2.4.9)$$

which, with the use of the boundary conditions in equations (2.4.4) and (2.4.5), can be easily solved. As with the knife edge punch indentation, equating $w(x=r)=w_o$ and solving for the load P one can minimize the loading with respect to the moving boundary of plastic deformation ζ to determine the maximum displacement w_o as a function of the plastic deformation ζ . In this way it can be found that for the hardening core response:

$$w_{Ho} = \frac{\bar{q}}{2k^2} \cdot e^{k(r-\zeta)} \left[e^{-k(r-\zeta)} - 1 \right]^2. \quad (2.4.10)$$

This solution can then be substituted into the previously found equation for the load P to arrive at an equation for the loading as a function of the plastic boundary ζ :

$$P_H = -\frac{\bar{q}}{k} \cdot N_o \cdot e^{k(r-\zeta)} \left\{ \left[1 - e^{-2k(r-\zeta)} \right] + k \cdot r \left[1 + e^{-2k(r-\zeta)} \right] \right\}. \quad (2.4.11)$$

In both equation (2.4.10) and equation (2.4.11) it can be shown that in the limit as $r \rightarrow 0$ and $E_i \rightarrow 0$ these equations reduce to the solutions found for the limiting condition.

Having solved for w_o and P as functions of the boundary ζ these functions can be substituted back into the solution for the deflection profile w , equation (2.4.9). This substitution significantly simplifies the constants C_1 and C_2 .

$$w_H = \frac{\bar{q}}{2k^2} \cdot e^{k(x-\zeta)} \left[e^{-k(x-\zeta)} - 1 \right]^2 \quad (2.4.12)$$

Further variable reduction can be achieved by normalizing the deflection profile w by the maximum displacement w_o , yielding the final normalized equation for the deflection of a hardening sandwich core under a rectangular punch indentation:

$$w_H^{norm} = e^{k(x-r)} \left[\frac{e^{k(\zeta-x)} - 1}{e^{k(\zeta-r)} - 1} \right]^2 \quad (2.4.13)$$

The same solution sequence can be employed for the sandwich core with a softening response to generate the following results:

$$w_S = C_1 \cdot e^{i \cdot kx} + C_2 \cdot e^{-i \cdot kx} + \frac{\bar{q}}{k^2}; \quad (2.4.14)$$

$$w_{So} = \frac{\bar{q}}{k^2} \left\{ 1 - \cos \left[k(r - \zeta) \right] \right\}; \quad (2.4.15)$$

$$P_S = \frac{2N_o\bar{q}}{k} \left\{ k \cdot r \cdot \cos \left[k(r - \zeta) \right] - \sin \left[k(r - \zeta) \right] - 2k \cdot r \right\}; \quad (2.4.16)$$

$$w_S = \frac{\bar{q}}{k^2} \left\{ 1 - \cos \left[k(x - \zeta) \right] \right\} \quad (2.4.17)$$

$$w_S^{norm} = \frac{\cos \left[k(x - \zeta) \right] - 1}{\cos \left[k(r - \zeta) \right] - 1}. \quad (2.4.18)$$

2.5 Comparison of Hardening Softening and Limiting Core Responses

In order to fully evaluate the solutions above it is essential to utilize a practical numerical example. Numerical evaluation will give a better understanding of how hardening and softening core constitutive equations affect the overall solution. To simplify the analysis several natural normalized parameters were defined based on the equations as follows:

$$\bar{\zeta} = \frac{\zeta}{\sqrt{h \cdot H}} \quad \bar{r} = \frac{r}{\sqrt{h \cdot H}} \quad \bar{w}_o = \frac{w_o}{H} \quad \bar{P} = \frac{P}{\sigma_o \sqrt{h \cdot H}}.$$

To enable numerical solution the following values were chosen:

$$\frac{r}{H} = 1 \quad \frac{H}{h} = 10 \quad \frac{E_t}{\sigma_o} = \frac{1}{100} \quad \frac{q_o}{E_t} = 1$$

These values are both practical in terms of magnitude and simplified to enable easy calculation. Beginning with the knife edge loading the parameters were normalized and the numerical values above were substituted into the equations of maximum displacement, and load-displacement to arrive at functions of $\bar{\zeta}$, the normalized moving plastic boundary.

**Comparison of Maximum Deflection for Knife Edge Loading
- Hardening, Softening and Limiting Core Reactions-**

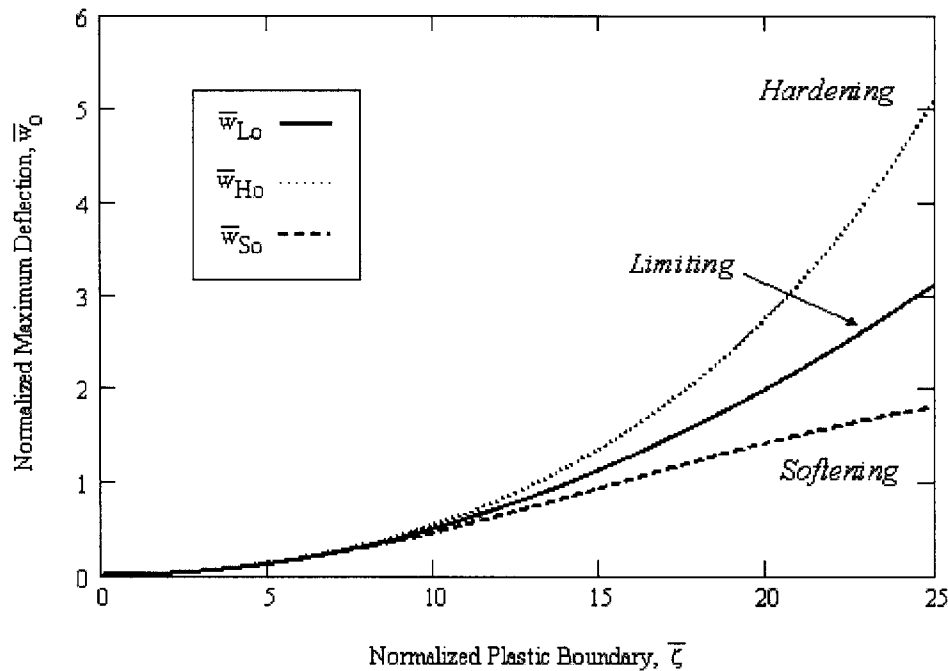


Figure 11 – Comparison of Maximum Deflections for Knife Edge Loading.

From figure 11 the differences in the maximum deflection of the face plate can be seen with increasing values for the normalized plastic boundary $\bar{\zeta}$. It is clearly demonstrated that for a

hardening response a larger maximum displacement would be required to produce the same amount of plastic deformation. Moreover, the function graphed for \bar{w}_{Ho} is an increasing exponential function which is what would be expected for a system in which hardening takes place with increased deformation. Conversely, the softening response in figure 11 demonstrates a decreasing trend as compared to the limiting case with increasing $\bar{\zeta}$.

Similarly, a plot of the normalized loading \bar{P} reveals the expected results; from figure 12 the loading required for increased plastic deformation increases for the hardening core reaction and decreases for the softening core reaction.

Comparison of Normalized Force for Knife Edge Loading - Hardening, Softening and Limiting Core Reactions -

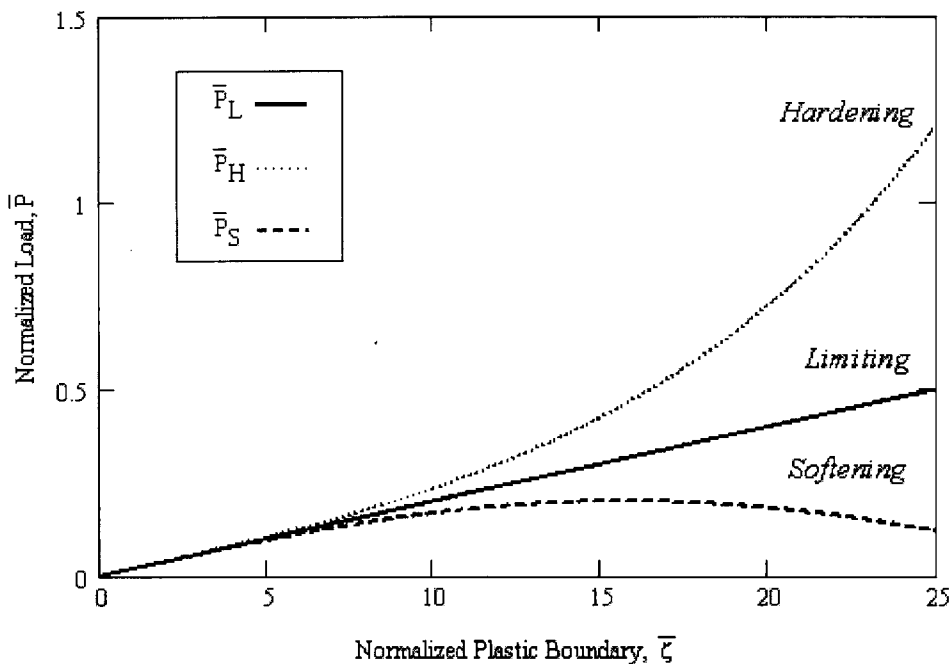


Figure 12 – Comparison of the Normalized Force for Knife Edge Loading.

An identical analysis can be conducted for the rectangular punch in which the maximum extent of deformation and loading are compared for hardening, softening and limiting core reactions. The presence of the rectangular punch limits the interval over which the equations are valid. That is, for values of $\bar{\zeta} < \bar{r}$ the equations are no longer valid and it is assumed that the face plate during deformation remains parallel to the rectangular punch as shown in figure 9. From the assumed physical values identified previously, $\bar{r} = \sqrt{10}$ and the evidence of the presence of this rectangular punch is readily seen in figure 13. Referring to the inset in figure 13, which is an exploded view of the functions, it can be seen that the three functions are essentially equal and the maximum deflection is zero at the point $\bar{\zeta} = \sqrt{10}$. For all values less than this the function is not valid and would be represented by zero as shown in the full size plot. In figure 13 it is once again obvious that the hardening core characteristically forces the maximum displacement to be larger for a given plastic deformation

while the softening core's deflection is less than the limiting case for the same plastic deformation.

The plot of the normalized loading \bar{P} versus the plastic boundary is shown in figure 14. Once again the hardening and softening functions are easily differentiated and show very similar natures, albeit offset and of much lower magnitudes, to those shown for the knife edge punch in figure 12. In figure 14 it is interesting to note that the plastic boundary initially sets itself up at a distance of approximately $2 \cdot \bar{r}$.

Comparison of Maximum Deflection for Rectangular Punch Loading - Hardening, Softening and Limiting Core Reactions-

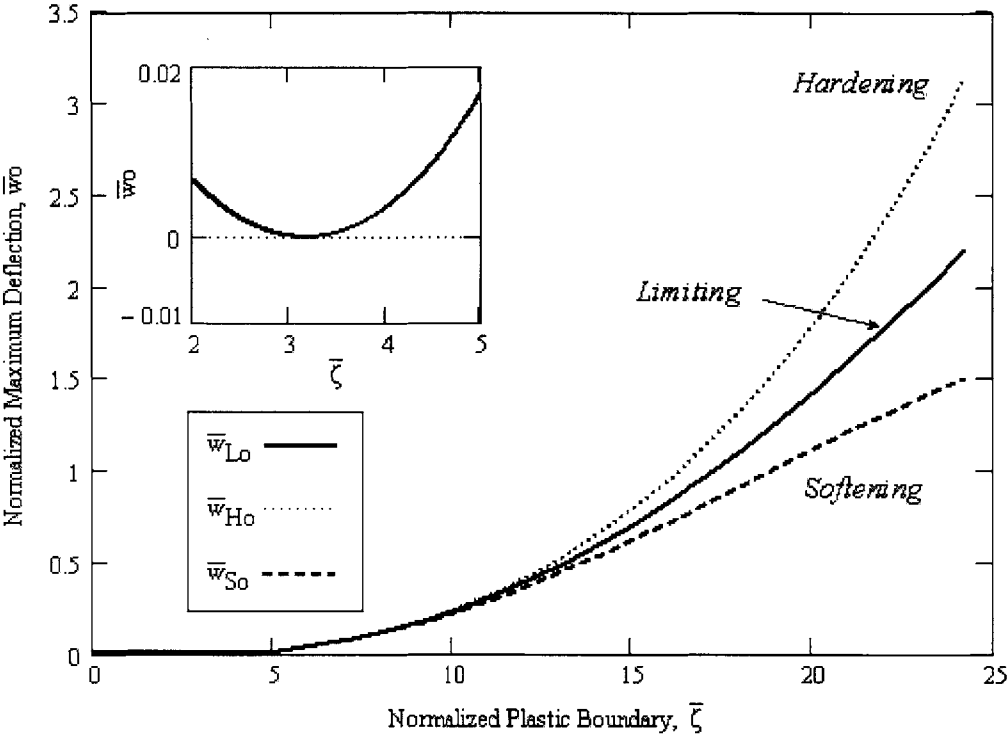


Figure 13 – Comparison of Maximum Deflection for Rectangular Punch Loading.

Comparison of Normalized Force for Rectangular Punch Loading - Hardening, Softening and Limiting Core Reactions-

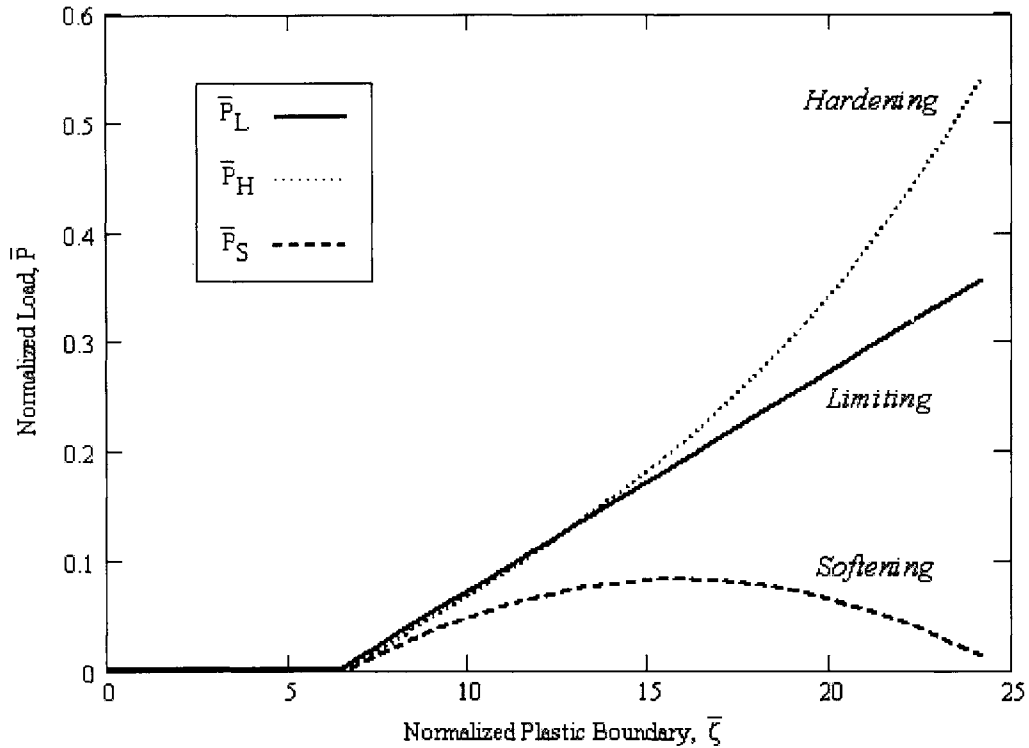


Figure 14 – Comparison of Normalized Force for Rectangular Punch Loading.

2.6 Parametric Analysis of Crush Response Models

The second investigation into the behavior of the crushing equations was a parametric study of the equation's reactions to varying material properties. This parametric study was conducted on the normalized deflection profiles to give a sense of the effect that increases in material properties have on the crushing of a sandwich panel. As with the analysis of the previous section a series of dimensionless parameters were defined

$$\bar{\zeta} = \frac{\zeta}{\sqrt{h \cdot H}} \quad \bar{r} = \frac{r}{\sqrt{h \cdot H}} \quad \bar{x} = \frac{x}{\sqrt{h \cdot H}}$$

and numerical values were assigned as follows:

$$\frac{r}{H} = 1 \quad \frac{H}{h} = 10 \quad \frac{\zeta}{r} = 1.96 \quad \frac{q_o}{E_t} = 1$$

From these assumptions the remaining variables in each of the normalized displacement profiles were \bar{x} and $K = E_t / \sigma_o$. By varying K , the only material property, a normalized side profile of the indentation could be produced over a range of values. Figure 15 and

PARAMETRIC ANALYSIS OF VARYING E_t/σ_o RATIO ON NORMALIZED DISPLACEMENT PROFILE
-- Rectangular Punch Indentation, Hardening --

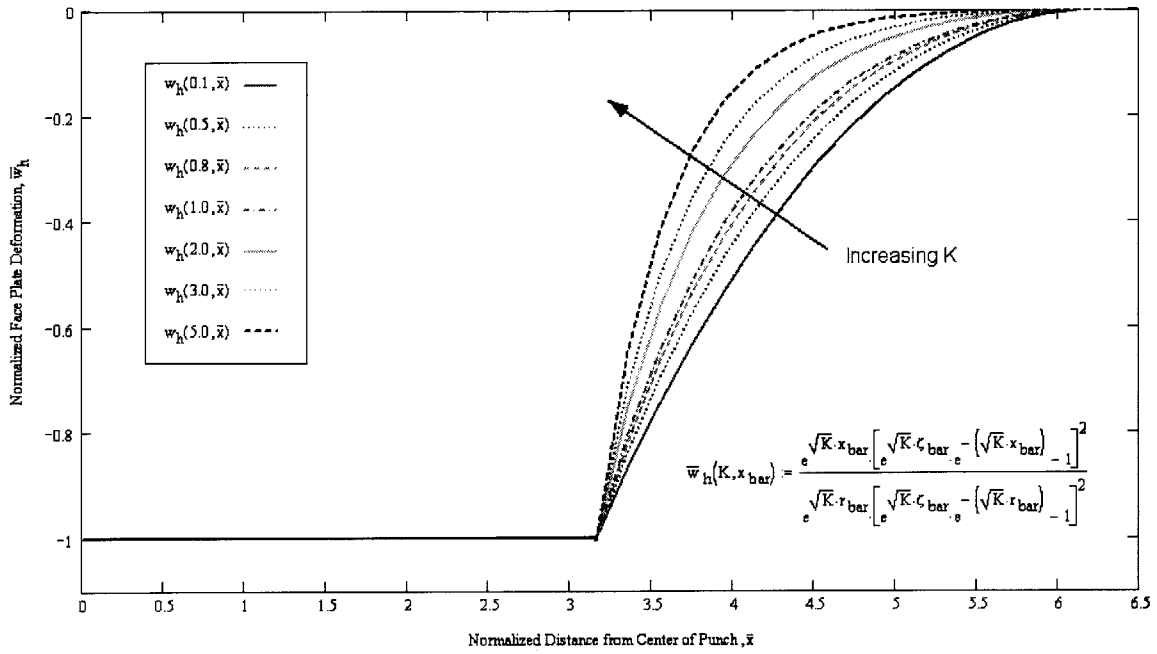


Figure 15 – Parametric Analysis of Varying E_t/σ_o for Hardening Core Response.

PARAMETRIC ANALYSIS OF VARYING E_t/σ_o RATIO ON NORMALIZED DISPLACEMENT PROFILE
-- Rectangular Punch Indentation, Softening --

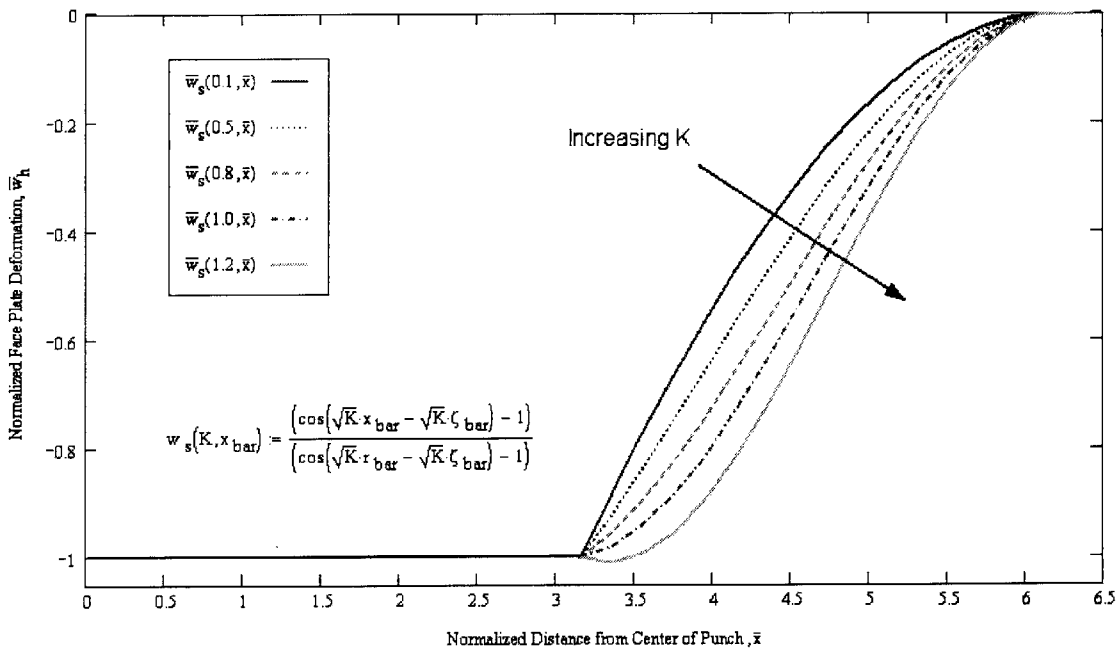


Figure 16 – Parametric Analysis of Varying E_t/σ_o for Softening Core Response.

figure 16 show the results of the variance of K in both the hardening and softening core response assumptions, respectively. Both plots strongly show the anticipated shape of asymptotic approach to zero deflection and a sharp discontinuity at $\bar{x} = \bar{r}$ ($\bar{r} = \sqrt{10}$ for this example). While the hardening core response's exponential dependence allows for a large variance in K the softening core response is limited by its periodic cosine dependence. It can be plainly seen in figure 16 that for a value of K greater than approximately 1.0 (as shown by the line furthest right in the figure) that the mathematical model no longer represents what we intuitively understand to occur. The sharp discontinuity at $\bar{x} = \bar{r}$ is inverted due to the periodicity of the cosine function and signals a breakdown of the equation's relevance.

2.7 Equation Summary

The two-dimensional crushing of a sandwich panel under quasi-static loading has been described. Utilizing a continuum constitutive model for the behavior of the core material, the following equations were derived to describe the plate's crushing behavior.

CHAPTER 2 – EQUATION SUMMARY	
LIMITING CASE	
$w_{Lo} = \frac{1}{2} \cdot \bar{q} \cdot \zeta^2$ $P_L = 2 \cdot N_o \cdot \bar{q} \cdot \zeta$ $w_L = \frac{1}{2} \cdot \bar{q} (x - \zeta)^2$ $w_L^{norm} = \frac{(x - \zeta)^2}{\zeta^2}$	
KNIFE EDGE PUNCH	
<u>Hardening Core Response</u> $w_{Ho} = \frac{\bar{q} (e^{k \cdot \zeta} - 1)^2}{2k^2 \cdot e^{k \cdot \zeta}}$ $P_H = \frac{\bar{q} \cdot N_o}{k} \cdot e^{k \cdot \zeta} (1 - e^{-2k \cdot \zeta})$ $w_H = \frac{\bar{q} \cdot e^{k(x-\zeta)}}{2k^2} (e^{-k(x-\zeta)} - 1)^2$ $w_H^{norm} = e^{kx} \cdot \frac{(e^{k(\zeta-x)} - 1)^2}{(e^{k\zeta} - 1)^2}$	<u>Softening Core Response</u> $w_{So} = \frac{\bar{q}}{k^2} (1 - \cos(k \cdot \zeta))$ $P_S = \frac{2N_o \cdot \bar{q}}{k} \cdot \sin(k \cdot \zeta)$ $w_S = \frac{\bar{q}}{k^2} \{1 - \cos[k(x - \zeta)]\}$ $w_S^{norm} = \frac{\cos[k(x - \zeta)] - 1}{\cos(k\zeta) - 1}$

Table 1 – Summary of Equations for Sandwich Plate Crushing

CHAPTER 2 – EQUATION SUMMARY, CON'T

RECTANGULAR PUNCH

Hardening Core Response

$$w_{Ho} = \frac{\bar{q}}{2k^2} \cdot e^{k(r-\zeta)} \left[e^{-k(r-\zeta)} - 1 \right]^2$$

$$P_H = -\frac{\bar{q}}{k} \cdot N_o \cdot e^{k(r-\zeta)} \left\{ \left[1 - e^{-2k(r-\zeta)} \right] + k \cdot r \left[1 + e^{-2k(r-\zeta)} \right] \right\}$$

$$w_H = \frac{\bar{q}}{2k^2} \cdot e^{k(x-\zeta)} \left[e^{-k(x-\zeta)} - 1 \right]^2$$

$$w_H^{norm} = e^{k(x-r)} \left[\frac{e^{k(\zeta-x)} - 1}{e^{k(\zeta-r)} - 1} \right]^2$$

Softening Core Response

$$w_{So} = \frac{\bar{q}}{k^2} \left\{ 1 - \cos \left[k(r - \zeta) \right] \right\}$$

$$P_S = \frac{2N_o\bar{q}}{k} \left\{ k \cdot r \cdot \cos \left[k(r - \zeta) \right] - \sin \left[k(r - \zeta) \right] - 2k \cdot r \right\}$$

$$w_S = \frac{\bar{q}}{k^2} \left\{ 1 - \cos \left[k(x - \zeta) \right] \right\}$$

$$w_S^{norm} = \frac{\cos \left[k(x - \zeta) \right] - 1}{\cos \left[k(r - \zeta) \right] - 1}$$

Table 1, Cont'd – Summary of Equations for Sandwich Plate Crushing

Chapter 3

CRUSH RESPONSE OF SUPPORTS

3.1 Introduction

The addition of crushable supports for the connection of the shell plating to the transverse bulkheads and decks is intended to reduce stress concentrations and to allow for load sharing between adjacent plate sections as well as to reduce the total load experienced by the plate. These crushable supports, an example of which is shown in figure 17, should delay the onset of fracture and increase the total energy absorbed in an accidental loading scenario.

Wierzbicki and Abramowicz [5] have proposed a series of analytical equations to describe the crushing of several different cross-sections. These equations have been validated with the use of extensive numerical modeling and will be used to describe the crush response of the proposed connection.

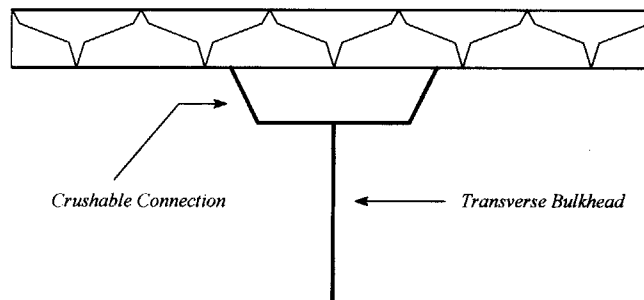


Figure 17 – Proposed Sandwich Panel Attachment Displaying Crushable Connection.

3.2 Analytical Solutions for Simple Cross-Sections

Wierzbicki and Abramowicz [3], Abramowicz [4] and Wierzbicki and Abramowicz [5] have described analytical solutions for the large strain, plastic deformation of thin walled structures. Some of the general shapes that were examined are shown in figure 18. In this project generic linear hardening and linear softening reactions, similar to those assumed for the core, will be investigated along with the analytical solutions for the un-braced circular and diamond cross-sections. These two shapes were chosen due to their relative similarity in response to what would be expected of the support modeled in figure 17 and their continuous nature. Moreover, the circular cross-section shows a clear hardening response while the diamond cross-section exhibits softening, thus they will provide good contrast to the assumed linear hardening and softening models. The square and rectangular cross-sections, along

with the braced sections, present varying modes or phases of failure and/or discontinuous crushing responses which unnecessarily complicate the mathematics.

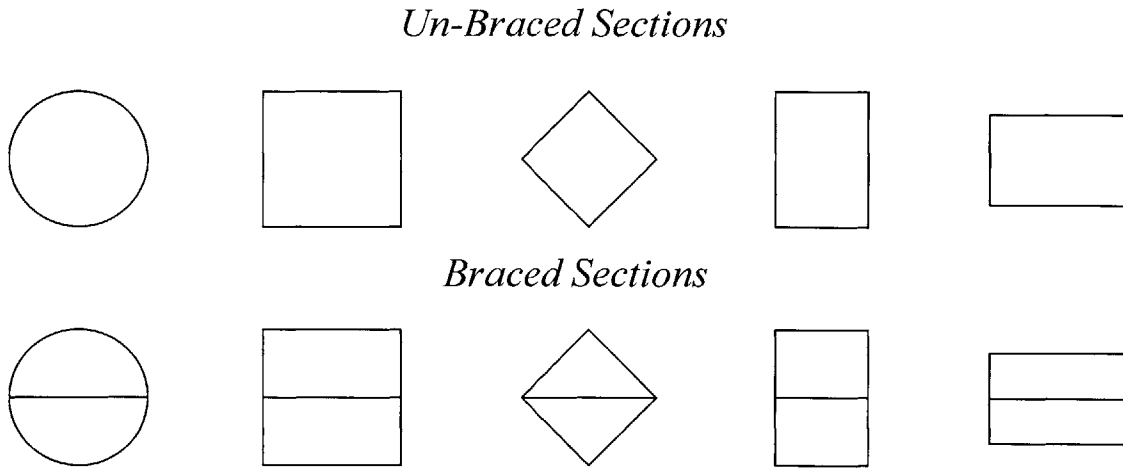


Figure 18 – Idealized Cross-Sections from Wierzbicki and Abramowicz [5].

The linear hardening and linear softening models are exactly the same as those presented for the core response of a sandwich panel; however, they are described as:

$$Q_1(w_2) = Q_o + k \cdot w_2 \quad (a)$$

$$Q_2(w_2) = Q_o - k \cdot w_2 \quad (b)$$

(3.2.1)

where Q_o is the initial rigidity and $\pm k$ is the constant hardening or softening for the crushing w_2 .

The crushing of a ring between two rigid plates was described by Wierzbicki and Abramowicz [3] based on a concept of moving plastic hinges. Their research led to the following load-displacement equation:

$$P = \frac{P_o}{\sqrt{1 - \frac{\delta}{2R}}} \quad \text{where,} \quad P_o = 2\pi \frac{M_o L}{R} \quad (3.2.2)$$

For this equation, $\delta = w_2$ and R is the radius of the ring. This equation provides a superior description of the actual ring resistance as compared to a solution utilizing stationary hinges as evidenced in figure 19 and figure 20. Figure 19 shows the difference between assumptions of moving or stationary hinges in the stiffening of a circular ring. The moving hinge creates a smooth curve (dashed line in figure 19) which agrees very well with the numerical solutions shown graphed in figure 20.

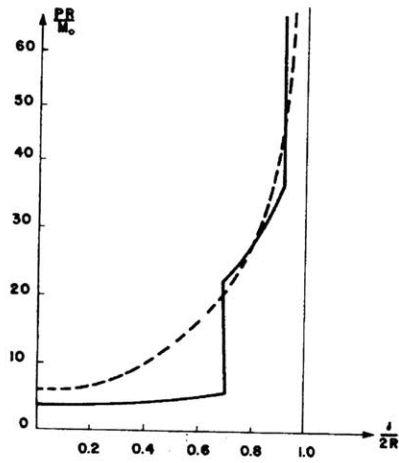


Figure 19 – Load-Displacement Characteristics of Rings with Stationary and Moving Hinges. From Wierzbicki and Abramowicz [3]

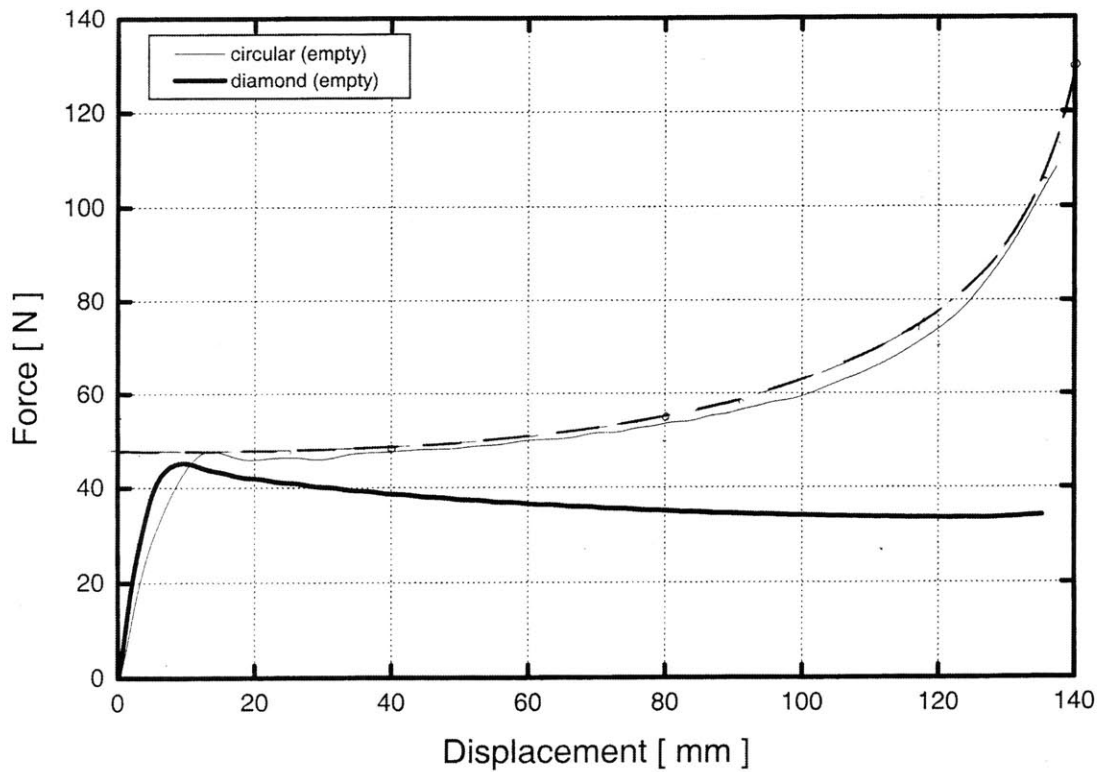


Figure 20 – Numerical Load-Displacement Versus Analytical Solution (Dashed Line) for Crushing of a Ring with Moving Hinges. From Wierzbicki and Abramowicz [5]

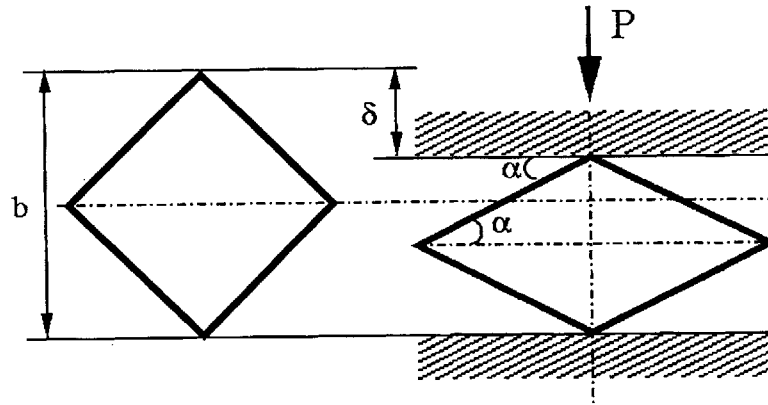


Figure 21 – Crushing of an Un-braced Diamond Cross Section. From Wierzbicki and Abramowicz [5].

The second shape of interest is the un-braced diamond. The analytical solution of the open diamond section was found from a collapse mechanism based on the assumption of four plastic hinges, one at each corner of the diamond, graphically represented in figure 21. The analytical equation for the crushing force was then shown to be:

$$P = \frac{P_o}{\sqrt{2 - \left(1 - \frac{\delta}{b}\right)^2}} \quad \text{where,} \quad P_o = 8 \frac{M_o L}{b} \quad (3.2.3)$$

The displacement δ is equal to w_2 in this analysis, while b indicates the initial height of the diamond which is also the maximum available crush distance. This equation shows a strong softening tendency as can be seen in figure 22 with the non-dimensionalized load decreasing from 1.0 to 0.707.

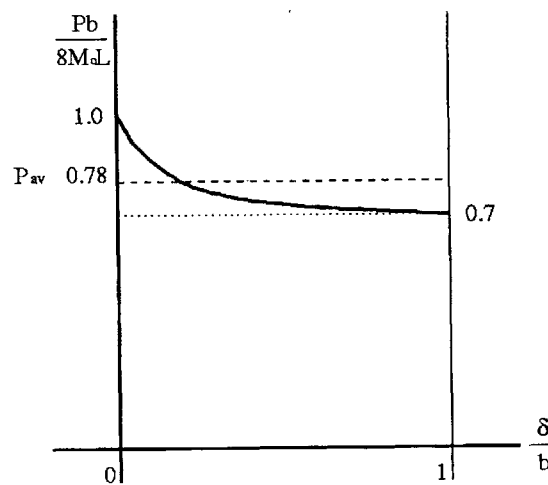


Figure 22 – Load-Displacement Curve for an Un-braced Diamond Cross-Section.

The crush response of the supports will be integrated independently into the beam and plate models discussed in the subsequent chapter. That is, the crushing of the springs will be assumed to occur independently of the sandwich beam/plate. In this way two load-displacement equations will be revealed to act simultaneously.

Chapter 4

MODELLING OF SUPPORTED SANDWICH PANEL

4.1 Introduction

The principal component of this research is to analytically quantify the effects of introducing a crushable connection between a double hull shell structure and its supporting transverse bulkheads. It is proposed that the addition of crushable connections will increase the amount of energy that can be absorbed by a ship's structure and, perhaps more importantly, crushable connections will help to delay the onset of fracture. As stated in the report's introduction, simple analytical techniques will be employed to explore the relative benefits of crushable connections. The aim of this report is neither to comment on the costs associated with the added complexity nor to address issues of producibility. Rather, the simplified analytical models will allow for tractable mathematics and readily achievable solutions that can be used to evaluate design merit as well as offering the possibility to aid in the validation finite element models.

Two approaches will be taken in the quantification of the effects of flexible connections: a two-dimensional beam or strip model of a sandwich plate on crushable supports; and a three-dimensional plastic analysis of a sandwich panel supported by crushable connections around its periphery. Xue and Hutchinson [6] have conducted numerical analysis on sandwich plate beam models and their results will provide a basis for validating the analytical results as well as allowing for a comparison between the load-displacement curves for rigidly and flexibly connected sandwich panels.

4.2 Standard Beam Bending Model

The beam model of a sandwich plate was created through the use of variational energy methods. The response was decomposed into a superposition of the membrane resistance of the face sheets, the constant shear resistance of the core modeled as a continuum and the crush resistance of the flexible bulkhead connections. The basic model is shown in figure 23. Each component of the internal energy absorbed can be separately derived, summed and then equated to the total external work done on the beam. Two independent displacement functions are assumed: one for the sandwich plate, w_1 ; and one for the crushable connections, w_2 . By assuming a symmetric linear deflection profile as shown by a dashed-line in figure 23, w_1 can be represented by:

$$w_1(x) = w_o \left(\frac{x}{L} - 1 \right) \quad (4.2.1)$$

where w_o is the maximum deflection for the plate at $x=0$. This form of the shape function $w_1(x)$ was chosen so as to produce a constant shear strain in the core material, reflecting the initial assumption of the core's reaction. Furthermore, if the core is assumed to experience

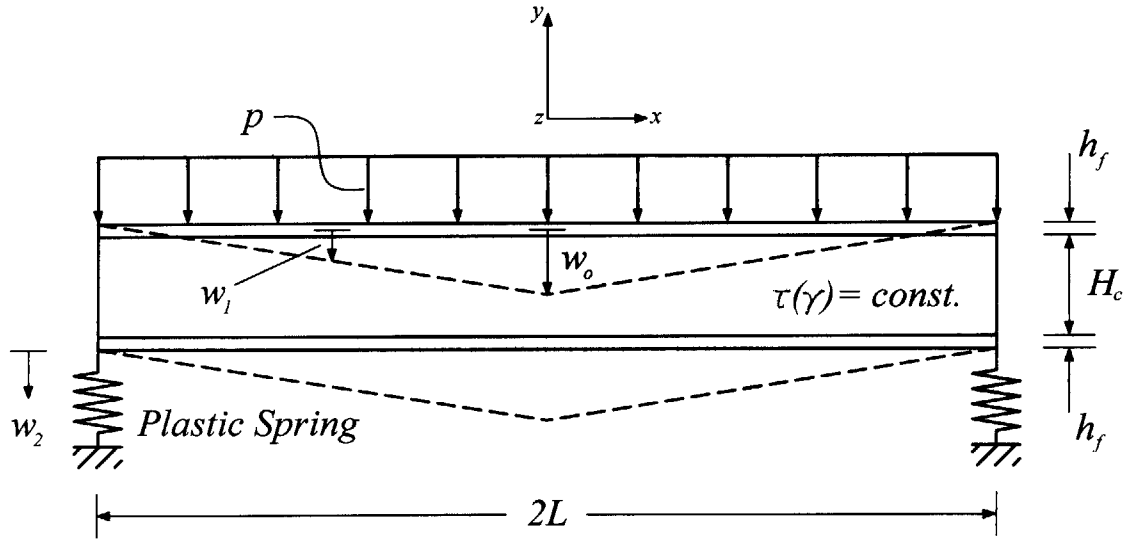


Figure 23 – Beam Bending Model.

only shearing and not crushing then a simple relation for the shear strain and its variation can be found from equation (4.2.1) to be:

$$\gamma = \frac{dw_1}{dx} = \frac{w_o}{L} \quad \delta\gamma = \frac{\delta w_o}{L} \quad (4.2.2)$$

Also using the assumed deformation the strain in the face plates due to membrane forces can be determined. Using an equation for arc length it can be shown that the strain in half of one of the face plates would be:

$$\varepsilon = \frac{1}{L} \int_0^L \frac{1}{2} \left(\frac{dw_1}{dx} \right)^2 dx. \quad (4.2.3)$$

Multiplying equation (4.2.3) by two to capture the symmetry of the plate, integrating and then differentiating with respect to time will yield the variational strain in a face plate to be:

$$\delta\varepsilon = 2 \left(\frac{w_o}{L} \right) \left(\frac{\delta w_o}{L} \right). \quad (4.2.4)$$

In order to formulate the total internal energy, each component described above must be included. The core will be approximated as providing a constant shear resistance, τ_o , the second component is the incremental energy associated with the membrane action of the face plates, while the crushing of the flexible connections will be approximated as plastic springs acting according to a general load-displacement function $Q(w_2)$. The variational internal energy was then written as:

$$\delta U = \iiint_{Vol} \tau_o \cdot \delta \gamma \cdot dV + \iiint_{Vol} \sigma_o \cdot \delta \varepsilon \cdot dV + \int_{Depth} Q(w_2) \cdot \delta w_2 \cdot dz \quad (4.2.5)$$

Substituting in equations (4.2.2) and (4.2.4) then integrating over the beam as shown in figure 23, the total variational internal energy becomes:

$$\delta U = (2H_c \tau_o) \delta w_o + \left(8 \frac{h_f}{L} \sigma_o w_o \right) \delta w_o + 2 \cdot Q(w_2) \delta w_2 \quad (4.2.6)$$

The external energy expended on deforming the beam is entirely due to the constant distributed load P . The variational external energy can be written as:

$$\delta V = \iint_{Area} p \cdot \delta v \cdot dA \quad (4.2.7)$$

In equation (4.2.7) v is the total vertical displacement which is the sum of w_1 and w_2 ; therefore, the variation of v will be:

$$\delta v = \delta w_o \left(\frac{x}{L} - 1 \right) + \delta w_2 \quad (4.2.8)$$

By substituting equation (4.2.8) into equation (4.2.7) and integrating over the area for which p acts, the total external work is:

$$\delta V = 2p \left(-\frac{L}{2} \right) \delta w_o + 2pL \cdot \delta w_2 \quad (4.2.9)$$

Equating the internal energy (equation (4.2.6)) to the external energy (equation (4.2.9)) and grouping similar terms, two independent equations for the load-displacement behavior of the beam model are achieved. The deflection of the sandwich plate is described by:

$$p_p = \left(8 \sigma_o \frac{h_f}{L^2} \right) w_o + 2 \tau_o \frac{H_c}{L}. \quad (4.2.10)$$

While the crushing of the flexible connections modeled as plastic springs is:

$$p_s = \frac{Q(w_2)}{L} \quad (4.2.11)$$

To investigate the validity of this model, the results for the load-displacement function for the sandwich plate, equation (4.2.10), were compared against numerical data published by Xue and Hutchinson [6]. They produced constitutive stress-strain diagrams for various core configurations. Utilizing the available data for a square honeycomb core illustrated in figure 24 the constant core shear was modeled using upper and lower bounds of

$$\text{Upper Bound: } \frac{\bar{\sigma}_{12}(\varepsilon_{ep})}{\bar{\sigma}_{12}(0)} = 2.15$$

$$\text{Lower Bound: } \frac{\bar{\sigma}_{12}(\varepsilon_{ep})}{\bar{\sigma}_{12}(0)} = 1.1$$

$$\text{Where from the report: } \bar{\sigma}_{12}(0) = 2.367 \text{ MPa}$$

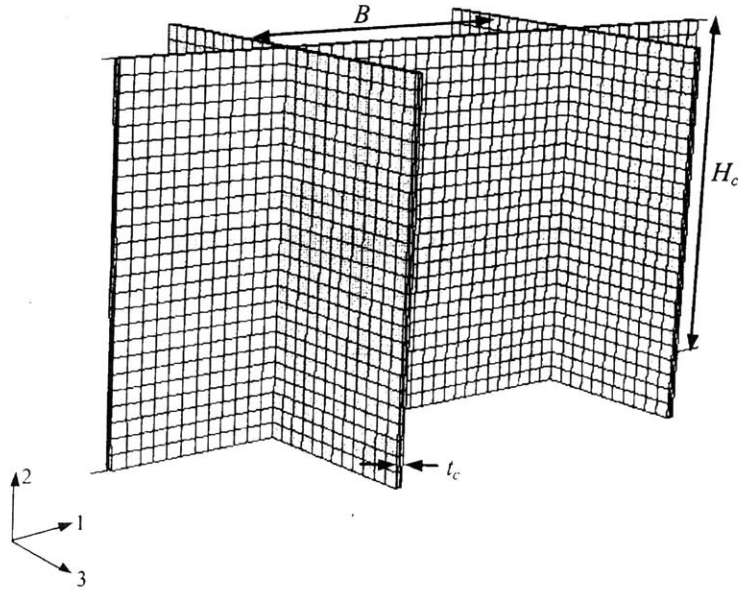


Figure 24 – Description of Modeled Square Honeycomb Core. From Xue and Hutchinson [6].

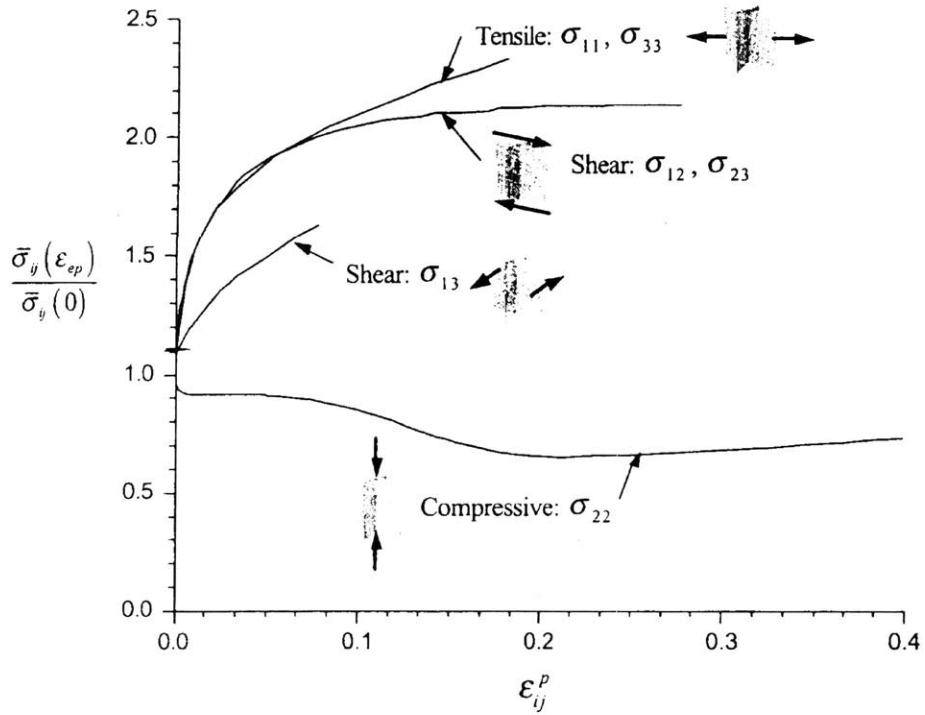


Figure 25 – Stress-Strain Representation of Honeycomb Core. From Xue and Hutchinson [6].

taken from the equivalent plot of core properties in figure 25. Assuming pure shearing the plastic shear stress will be $\bar{\sigma}_{12}(\varepsilon_{cp}) = \sqrt{3} \bar{\sigma}_{12}$; therefore, the lower and upper bound shear stresses become:

$$\bar{\sigma}_{12}^{Upper} = 2.938 \text{ MPa} \quad \bar{\sigma}_{12}^{Lower} = 1.503 \text{ MPa}$$

Utilizing these values for τ_o in equation (4.2.10) a plot of the load-displacement curve was made. In order to facilitate comparison with Xue and Hutchinson's data the load p_p must be normalized by a reference pressure defined by Xue and Hutchinson [6] as:

$$p_c = \sigma_y \frac{(2h_f + \bar{\rho}_c H_c)^2}{L^2}, \quad (4.2.12)$$

which represents the limiting pressure in bending of a solid, clamped, elastic-perfectly plastic plate having the same mass per area as the sandwich plate where $\bar{\rho}_c$ is the relative density of the core. For their given model defined as:

$$304 \text{ Stainless Steel : } \sigma_y = 205 \text{ MPa} \quad \frac{H_c}{L} = 0.1 \quad \frac{h_f}{H_c} = 0.08 \quad \bar{\rho}_c = 0.04$$

equation (4.2.10) reduces to:

$$\begin{aligned} \frac{p_s^{Upper}}{p_c} &= 160 \left(\frac{w_o}{L} \right) + 7.17 & (a) \\ \frac{p_s^{Lower}}{p_c} &= 160 \left(\frac{w_o}{L} \right) + 3.67 & (b) \end{aligned} \quad (4.2.13)$$

These two linear functions are plotted against the published results in figure 26. Examining figure 26 on the following page it is initially clear that the slope of the upper and lower bound lines are very similar to that produced by Xue and Hutchinson [6] using extensive numerical modeling. The slope is entirely a function of the membrane stress, as can be seen in equation (4.2.10), and thus it's similarity to Xue and Hutchison's model is a testament to the extent that membrane forces dominate the process. The initial rigidity of the upper and lower bounds is slightly larger than the initial elastic phase shown by Xue and Hutchinson.

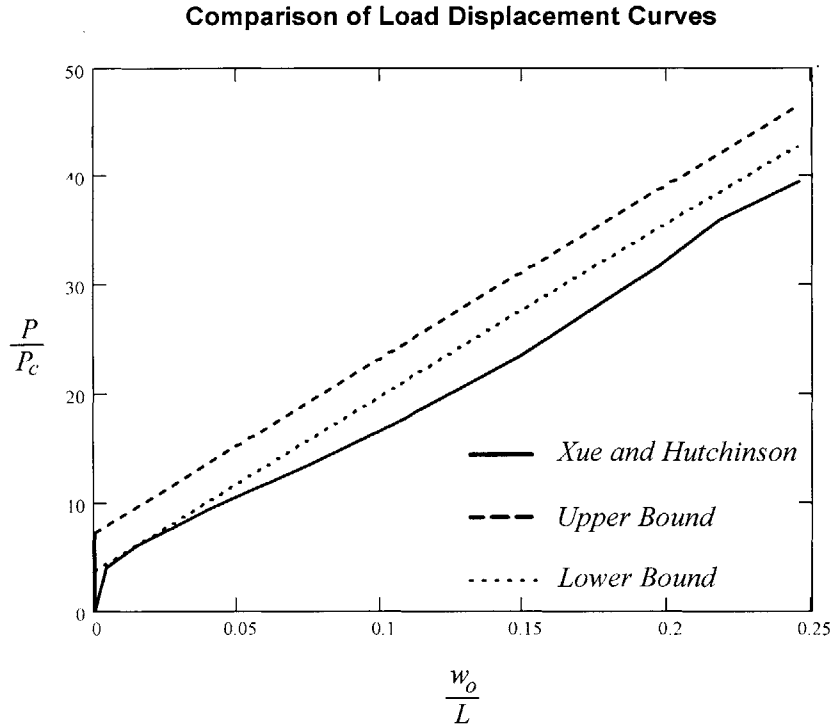


Figure 26 – Comparison of Load Displacement Curves.

4.3 Plate Bending Model With Crushable Connections

Expanding on the beam analysis, the model was increased to a three-dimensional description of a sandwich plate undergoing plastic deformation. The proposed mathematical model is shown in figure 27 where the sandwich plate is supported on all four edges by plastic springs and is exposed to a constant distributed load over the upper face plate.

Mathematically, the three-dimensional plate deformation model was described using variational energy methods by equating a superposition of plate resistance to bending and stretching, core shear reaction resistance and the resistance of the crushable connections to the external energy produced by the deformation force. It was assumed that the top and bottom plates deformed under a fully plastic regime described by fixed plastic hinges and rigidly rotating plates. As with the beam model, the resistance from the core was assumed to be entirely a result of shearing within the core. As a result of this assumption, the distance between the upper plate and lower plate remains constant throughout the deformation incident as described by this mathematical model.

The energy absorbed by the deformation of the upper and lower face plates was calculated through the use of a failure mechanism similar to one postulated by plastic hinge-line theory. A thesis by Wiernicki [7] has an exceptionally thorough derivation for the internal energy absorbed by a plate undergoing deformation as shown in figure 28. For this model, the plate is clamped along all edges causing the large plastic deflections to be

dominated by membrane stretching. Furthermore, the elastic deformation of the plate is taken to be negligible resulting in the material being approximated as rigid-perfectly plastic.

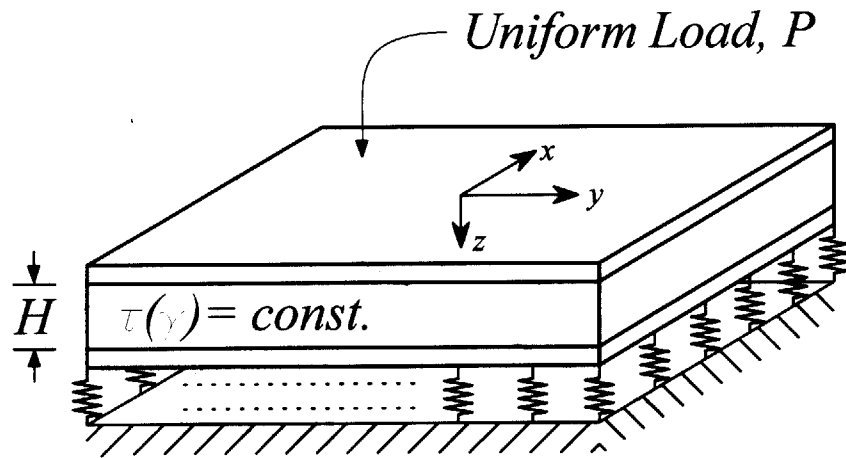


Figure 27 – Theoretical Set-up for a Sandwich Plate on Crushable Supports.

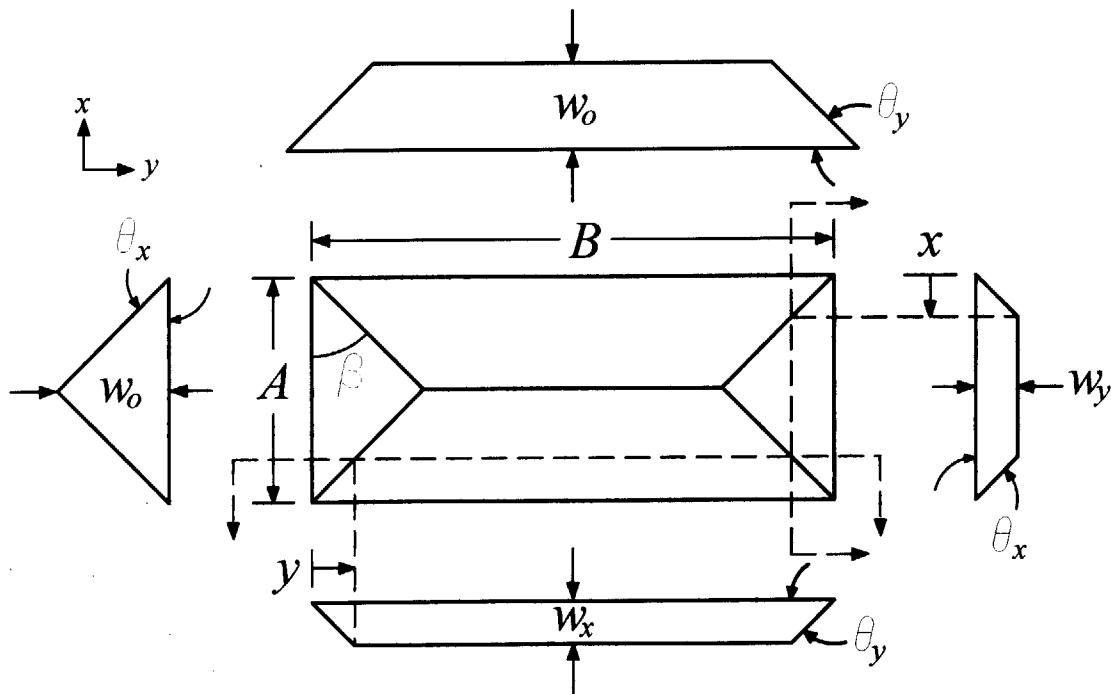


Figure 28 – Assumed Plastic Hinge-Line Deformation.

In Wiernicki [7], the four plate areas remain flat while all deformation occurs in the plastic hinge lines which are assumed to be straight. The moment behavior is then uncoupled from the membrane forces in each direction, thus allowing the internal energy dissipated within the plate to be decomposed into a summation of the x- and y-components of the energies of each plastic hinge. With these simplifications it can be shown that the increment of internal energy dU along an increment of hinge line dl is:

$$\delta U = (M_{o_x} \delta \theta_x \sin \beta + N_{o_x} w \delta \theta_x \sin \beta) dl + (M_{o_y} \delta \theta_y \cos \beta + N_{o_y} w \delta \theta_y \cos \beta) dl \quad (4.3.1)$$

where,

M_{o_x}, M_{o_y} - Yield Moments in x- and y-directions;

N_{o_x}, N_{o_y} - Membrane Yield Moments in x- and y-directions;

w - Vertical plate displacement as a function of x and y; max deflection = w_o .

The solution for the internal energy dissipated through this plastic deformation can be further decomposed into a superposition for each of the five hinge-lines and four boundary lines.

The internal energy dissipated in of each of the four angled lines will be a summation of the x- and y-components for each hinge-line. Beginning with the x-direction: for one of the angled hinges:

$$\delta U_{x,ANGLE} = (M_{o_x} \delta \theta_x \sin \beta + N_{o_x} w_x \delta \theta_x \sin \beta) dl \quad (4.3.2)$$

where, substituting in:

$$\delta \theta_x = \frac{2\delta w_o}{A} \quad w_x = \left(\frac{2w_o}{A} \right) x \quad dl = \frac{dx}{\cos \beta}$$

and integrating over the interval from $x=0$ to $x=A/2$ yields,

$$\delta U_{x,ANGLE} = M_{o_x} \delta w_o \left(\tan \beta + \frac{N_{o_x}}{M_{o_x}} \frac{w_o}{2} \tan \beta \right) \quad (4.3.3)$$

Since the assumed problem is symmetric the energy dispersed in each of the angled hinges in the x-direction will be equal; therefore, the x-component of the total internal energy absorbed by the angled hinges will simply be four times equation (4.3.3):

$$\delta U_{x,ANGLE} = 4M_{o_x} \delta w_o \left(\tan \beta + \frac{N_{o_x}}{M_{o_x}} \frac{w_o}{2} \tan \beta \right) \quad (4.3.4)$$

Similarly in the y-direction, the increment of internal energy will be:

$$\delta U_{y,ANGLE} = (M_{o_y} \delta \theta_y \cos \beta + N_{o_y} w_y \delta \theta_y \cos \beta) dl \quad (4.3.5)$$

substituting,

$$\delta \theta_y = \frac{2\delta w_o}{A \cdot \tan \beta} \quad w_y = \left(\frac{2w_o}{A \cdot \tan \beta} \right) y \quad dl = \frac{dy}{\sin \beta}$$

integrating and multiplying by four to capture the symmetry of the deformation, the y-component of the internal energy absorption of angled hinges will be:

$$\delta U_{y_ANGLE} = 4M_{o_y} \delta w_o \left(\frac{1}{\tan \beta} + \frac{N_{o_x} w_o}{M_{o_x}} \cdot \frac{1}{2 \tan \beta} \right). \quad (4.3.6)$$

The energy dispersion component of the centerline hinge where $\beta=90^\circ$ and $w=w_o$ is described by:

$$\delta U_{CENTER} = (M_{o_x} \delta \theta_x + N_{o_x} w_x \delta \theta_x) dl \quad (4.3.7)$$

Here, at the centerline hinge, the angle is $180^\circ - 2\theta_x$ as deformation occurs symmetrically on both sides of the centerline, therefore, using

$$\delta \theta_x = \frac{4\delta w_o}{A} \quad dl = dy$$

equation (4.3.7) reduces to:

$$\delta U_{CENTER} = \left(M_{o_x} \frac{4\delta w_o}{A} + N_{o_x} w_o \frac{4\delta w_o}{A} \right) dy \quad (4.3.8)$$

In order to determine the total internal energy equation (4.3.8) must be integrated over the length of the centerline, which can be shown to be $B - A \cdot \tan \beta$. This produces the following equation for the internal energy dissipated along the centerline hinge:

$$\delta U_{CENTER} = 4M_{o_x} \delta w_o \left[\frac{B}{A} - \tan \beta + \frac{N_{o_x} w_o}{M_{o_x}} \left(\frac{B}{A} - \tan \beta \right) \right] \quad (4.3.9)$$

The boundaries can be divided into boundaries extending in the y-direction and boundaries extending in the x-direction. For the boundaries extending in the x-direction $\beta=0^\circ$ and $w=0$. This consequently reduces equation (4.3.1) to

$$\delta U_{x_BOUND} = (M_{o_y} \delta \theta_y) dl \quad (4.3.10)$$

By defining the following

$$\delta \theta_y = \frac{2\delta w_o}{A \cdot \tan \beta} \quad dl = dx$$

and integrating over the length of the boundary ($-A/2$ to $A/2$), the energy dissipated within one boundary line will be:

$$\delta U_{x_BOUND} = \frac{2M_{o_y}}{\tan \beta} \delta w_o \quad (4.3.11)$$

As with the angled hinge-lines the energy dissipated in the two parallel boundary lines running in the x-direction will be equal. Thus, multiplying equation (4.3.11) by two gives the total internal energy dissipated within the x-direction boundary hinge-lines as:

$$\delta U_{x_BOUND} = \frac{4M_{o_y}}{\tan \beta} \delta w_o \quad (4.3.12)$$

For the y-direction boundaries where $\beta=90^\circ$ and $w=0$ the increment of internal energy can be written as:

$$\delta U_{y_{BOUND}} = (M_{o_x} \delta \theta_x) dl \quad (4.3.13)$$

where,

$$\delta \theta_x = \frac{2\delta w_o}{A} \quad dl = dy$$

Once again due to symmetry the total energy dissipated by the two parallel boundaries will be equal, thus doubling equation (4.3.13) and integrating over the interval from $-B/2$ to $B/2$ gives:

$$\delta U_{y_{BOUND}} = 4M_{o_x} \delta w_o \frac{B}{A} \quad (4.3.14)$$

Now that each individual component of the deformed plate's energy absorption is solved for, equations (4.3.4), (4.3.6), (4.3.9), (4.3.12), and (4.3.14) can be summed to arrive at the total incremental internal energy absorption for a plate undergoing plastic deformation as shown in figure 28. Furthermore, since the sandwich panel is constructed of upper and lower face plates, each deforming identically, the total energy for both plates will be twice that of a single plate; therefore:

$$\begin{aligned} \delta U_{PLATE} &= \delta U_{x_{ANGLE}} + \delta U_{y_{ANGLE}} + \delta U_{CENTER} + \delta U_{x_{BORDER}} + \delta U_{y_{BORDER}} \\ \delta U_{PLATE} &= 2 \cdot \delta w_o \left\{ \left[8M_{o_x} \frac{B}{A} + \frac{8M_{o_y}}{\tan \beta} \right] + 2w_o \left[N_{o_x} \left(2\frac{B}{A} - \tan \beta \right) + \frac{N_{o_y}}{\tan \beta} \right] \right\}. \quad (4.3.15) \end{aligned}$$

By assuming that each plate is isotropic, $M_{o_x} = M_{o_y} = M_o$ and $N_{o_x} = N_{o_y} = N_o$, then equation (4.3.15) can be reduced to its final form:

$$\delta U_{PLATE} = 2 \cdot \delta w_o \left[8M_o \left(\frac{B}{A} + \frac{1}{\tan \beta} \right) + 2N_o w_o \left(2\frac{B}{A} - \tan \beta + \frac{1}{\tan \beta} \right) \right] \quad (4.3.16)$$

Having determined the total energy dissipation contributed by the deformation of the two face plates, the reaction due to the presence of the core can be investigated. Similar to the beam model the core is assumed to contribute only through shear, thus there is no crushing of the core taken into account. This approximation is valid for cores which exhibit very low in plane shear resistance and whose crushing reaction will be negligible compared to the membrane forces created in the face sheets. By assuming a constant shear resistance τ_o and identifying four zones in which shearing occurs a relationship for the energy dispersed through shearing can be formed; the zones correspond to the assumed deflection profile for the sandwich panel. Figure 29 illustrates the core shearing zones and the related shear components associated with each along with a plot of the assumed constant shear resistance. Utilizing the same nomenclature displayed in figure 28 the shear strain components γ_{xz}

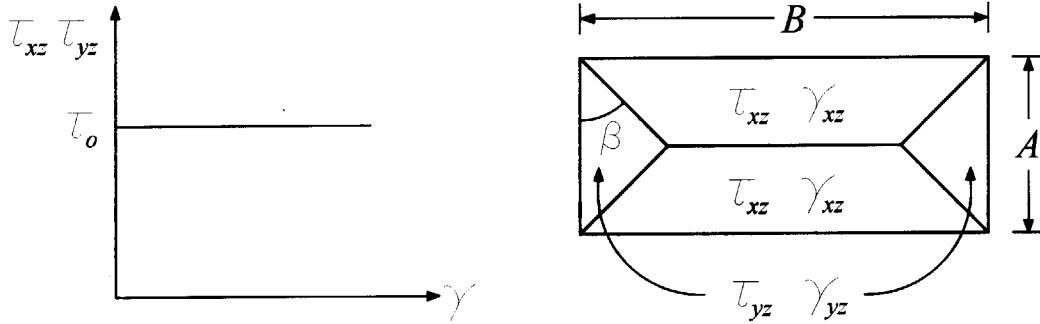


Figure 29 – Assumed Shear Response and Related Shear Zones of Core.

and γ_{yz} can be solved for. Assuming $\gamma_{xz} \approx \theta_x$ and $\gamma_{yz} \approx \theta_y$ it can be shown that:

$$\gamma_{xz} = \frac{2w_o}{A} \quad \text{and} \quad \gamma_{yz} = \frac{2w_o}{A \cdot \tan \beta} \quad (4.3.17)$$

The energy dissipated within the core due to shear resistance can be solved from:

$$\delta U_{CORE} = \iiint_V (\tau_{xz} \delta \gamma_{xz} + \tau_{yz} \delta \gamma_{yz}) dV \quad (4.3.18)$$

Once again taking advantage of symmetry there are two sets of identical zones, shown in figure 29 as isosceles trapezoids and triangles, thus equation (4.3.18) can be divided into two separate integrations over these areas. In addition by using equation (4.3.17) and setting $\tau_{xz} = \tau_{yz} = \tau_o$ the internal energy dispersed by the core becomes:

$$\delta U_{CORE} = 2 \iiint_{Triangle} \left(\tau_o \frac{2}{A \cdot \tan \beta} \delta w_o \right) dV + 2 \iiint_{Trapezoid} \left(\tau_o \frac{2}{A} \delta w_o \right) dV \quad (4.3.19)$$

The integration over the triangular zone can be performed over the following ranges and doubled:

$$\begin{aligned} x: & 0 \rightarrow \frac{A}{2} - \frac{y}{\tan \beta} \\ y: & 0 \rightarrow \frac{A}{2} \cdot \tan \beta \\ z: & 0 \rightarrow H \end{aligned}$$

while the trapezoid can be integrated over the following ranges and doubled:

$$\begin{aligned} x: & 0 \rightarrow \frac{A}{2} \\ y: & 0 \rightarrow \frac{B}{2} - x \cdot \tan \beta . \\ z: & 0 \rightarrow H \end{aligned}$$

Performing the integration over the prescribed intervals yields the final equation for the contribution from the core due to shear,

$$\delta U_{CORE} = HA \cdot \tau_o \cdot \delta w_o \left(1 + 2 \frac{B}{A} - \tan \beta \right) \quad (4.3.20)$$

The final element to add to the internal energy dissipation equation is the contribution due to the crushable connections, illustrated as plastic springs in figure 27. The addition of these crushable supports is the central improvement to this quasi-static model. It is anticipated that the extra energy absorption provided by the crushable supports will aid in the practical delay of fracture and increase the overall loading that a sandwich panel may experience prior to punch through. For a simplified representation, the plastic springs will be modeled as initially rigid, transitioning to a linearly softening plastic deformation as shown in figure 30; however, any of the models described in Chapter 3 would be appropriate. In

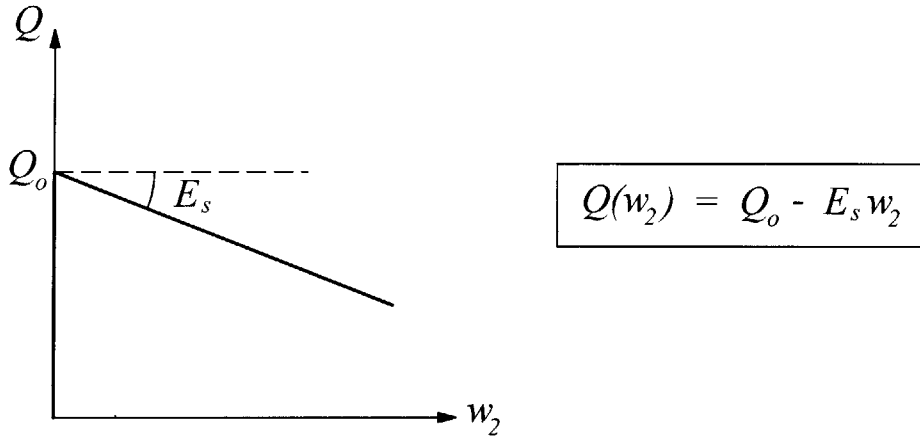


Figure 30 – Assumed Softening Response and Equation for Crushable Connections.

order to accommodate this secondary crushing mechanism a second displacement w_2 is added to reflect the extent of crush experienced by the plastic springs in the z -direction. The energy dissipated or absorbed by the crushing of the plastic springs is described by:

$$\delta U_{SPRINGS} = \oint [Q(w_2) \cdot \delta w_2] dl \quad (4.3.21)$$

Using the equation for the reaction of the crushable spring in figure 30, and the notation from figure 28, equation (4.3.21) becomes:

$$\delta U_{SPRINGS} = 2 \left[\int_{-A/2}^{A/2} (Q_o - E_s w_2) \cdot \delta w_2 dx + \int_{-B/2}^{B/2} (Q_o - E_s w_2) \cdot \delta w_2 dy \right] \quad (4.3.22)$$

Integrating equation (4.3.22) will produce the final solution for the additional energy absorbed by the crushable supports:

$$\delta U_{SPRINGS} = \delta w_2 \left[2(A+B)(Q_o - E_s w_2) \right] \quad (4.3.23)$$

Having determined each component of the internal energy, the total internal energy dissipated can be calculated as the summation of each component. That is,

$$\delta U_{TOTAL} = \delta U_{PLATE} + \delta U_{CORE} + \delta U_{SPRINGS} \cdot \quad (4.3.24)$$

Substituting equations (4.3.16), (4.3.20), and (4.3.23) into equation (4.3.24) yields the final equation for the total internal energy for this system:

$$\begin{aligned} \delta U_{TOTAL} = & \left[16M_o \left(\frac{B}{A} + \frac{1}{\tan \beta} \right) + 4N_o w_o \left(2 \frac{B}{A} - \tan \beta + \frac{1}{\tan \beta} \right) \right] \delta w_o \\ & + \left[HA \cdot \tau_o \left(1 + 2 \frac{B}{A} - \tan \beta \right) \right] \delta w_o \\ & + \left[2(A+B)(Q_o - E_s w_2) \right] \delta w_2 \end{aligned} \quad (4.3.25)$$

To complete the analysis the internal energy must be balanced by the external energy input into the system. The external work is produced by a constant distributed load acting on the face of the sandwich plate and moving through a $w(x,y)$ as the plate deforms and w_2 as the supports collapse. The variation of external energy can therefore be written as a sum of the contributions due to the deformation of the plate and due to the deformation of the supports:

$$\delta V = \iint_A P \delta w dA + \iint_A P \delta w_2 dA \quad (4.3.26)$$

For constant external pressure P and using the deformed shape of the plate as shown in figure 28, equation (4.3.26) becomes:

$$\delta V = \frac{PA^2}{6} \left(3 \frac{B}{A} - \tan \beta \right) \delta w_o + PAB \cdot \delta w_2 \quad (4.3.27)$$

By equating the total internal energy dissipated with the total external work, a relationship for the load-displacement behavior of the present model can be found. Therefore, equating (4.3.25) to (4.3.27) and matching terms based on the variational displacements δw_o and δw_2 two equations are produced:

$$P_p = \frac{96M_o \left(B + \frac{A}{\tan \beta} \right) + 6HA \cdot \tau_o (A + 2B - A \tan \beta) + 24N_o \left(2B - A \tan \beta + \frac{A}{\tan \beta} \right) w_o}{A^2 (3B - A \tan \beta)} \quad (4.3.28)$$

$$P_s = 2 \frac{(A+B)}{AB} (Q_o - E_s w_2) \quad (4.3.29)$$

where P_p represents the load displacement function for the sandwich plate while P_s is equal to the load displacement function of the crushable connections. Both equation (4.3.28) and

equation (4.3.29) are linear functions of displacements w_o and w_2 , respectively. Therefore, rearranging the equations to clarify:

$$P_p = \left[\frac{24N_o \left(2B - A \tan \beta + \frac{A}{\tan \beta} \right)}{A^2 (3B - A \tan \beta)} \right] w_o + \left[\frac{96M_o \left(B + \frac{A}{\tan \beta} \right) + 6HA \cdot \tau_o (A + 2B - A \tan \beta)}{A^2 (3B - A \tan \beta)} \right] \quad (4.3.30)$$

$$P_s = \left[2 \frac{(A+B)}{AB} Q_o \right] - \left[2 \frac{(A+B)}{AB} E_s \right] w_2. \quad (4.3.31)$$

4.4 Analysis of Quasi-Static Load Response

Further analysis of the models will continue with the beam bending model. Since the plate model outlined in the previous section decomposes into two independent, linear functions of w_1 and w_2 , the same form as for the beam model, the basic mathematics will develop in the same manner although carrying many more variables. Since the goal of this thesis was not to design the connections themselves, but rather to conduct simple analytical investigations into the general behavior of the proposed system, the load-displacement functions will also remain general. Therefore, to explore the potential benefits of including a crushable connection the beam model will be used in conjunction with the four general load-displacement functions $Q(w_2)$ described in Chapter 3. That is, linear hardening and linear softening functions were selected to form the basic, limiting conditions, while the more advanced analytical crush response models, based on numerical validation, were added to provide more insight into practical response characteristics. The load-displacement functions are described as follows:

$$\begin{aligned} (a) \quad \text{Linear Hardening:} \quad & Q_1(w_2) = Q_o + k \cdot w_2 \\ (b) \quad \text{Linear Softening:} \quad & Q_2(w_2) = Q_o - k \cdot w_2 \\ (c) \quad \text{Circular Cross-Section:} \quad & Q_3(w_2) = \frac{Q_o}{\sqrt{1 - \frac{w_2}{2R}}} \\ (d) \quad \text{Diamond Cross-Section:} \quad & Q_4(w_2) = \frac{Q_o}{\sqrt{2 - \left(1 - \frac{w_2}{b}\right)^2}} \end{aligned} \quad (4.4.1)$$

where, Q_o represents an initial rigidity. Equation (4.4.1)(c) was described in Chapter 3 as relating to the crushing of an open circular cross-section where $2R$ is the diameter of the circle or the total crushable height of the connection. Whereas equation (4.4.1)(d) is an analytical approximation for the crushing of a diamond section with an initial height, or total crushable height, b . Plots of these four functions are shown in figure 31 where the linear

hardening and softening responses increase or decrease, respectively, with a slope of k . figure 31(c) demonstrates a hardening response that asymptotically approaches the locking point at $w_2=2R$ and figure 31(d) is a softening response that locks at $w_2=b$. In order to retain

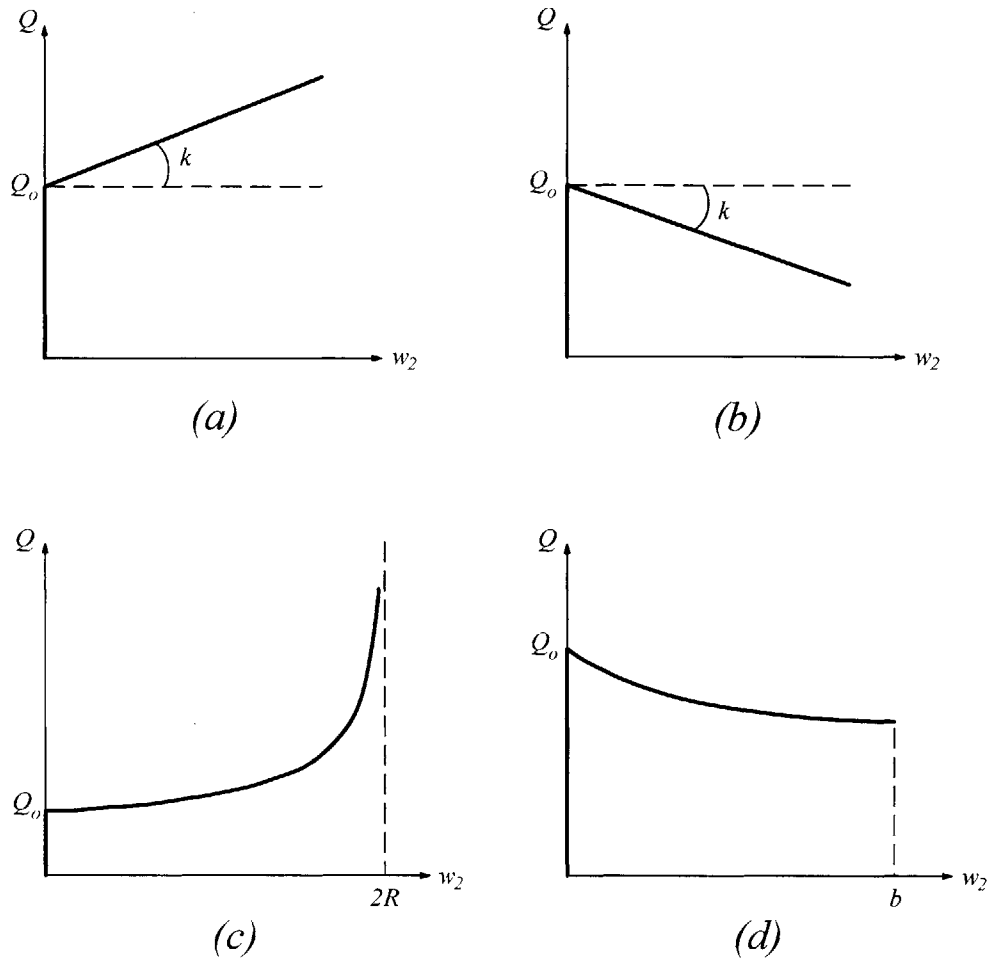


Figure 31 – Crushable Connection Load-Displacement Functions.

generality, the response of the three functions in equation (4.4.1) will be added to the sandwich panel's response in equation (4.2.10) for each of two cases:

$$\begin{aligned} \text{Case 1:} \quad & \frac{Q_0}{L} > 2\tau_o \frac{H_c}{L} \\ \text{Case 2:} \quad & \frac{Q_0}{L} < 2\tau_o \frac{H_c}{L} \end{aligned}$$

These cases will be described qualitatively and then a simple numerical example will compare the results to the previous model described in Section 3.2.

Beginning with the hardening response for **Case 1** in which $Q_0/L > 2\tau_o H_c/L$ it is obvious that the sandwich plate will begin to yield and deform prior to the crushable connections. With reference to figure 32, one can see that deformation of the sandwich plate

will continue until the load exceeds the initial rigidity of the connections at point (i). From this point on, continued increase in the applied load P will cause shared deformation between both the sandwich plate and the crushable connection until the crushable connection is fully collapsed. At this point the load carrying capacity of the connections themselves becomes infinite and their deformation w_2^{Spring} ceases. Therefore, at point (ii) the sandwich plate will once again carry the full load P and will continue to deform alone until fracture.

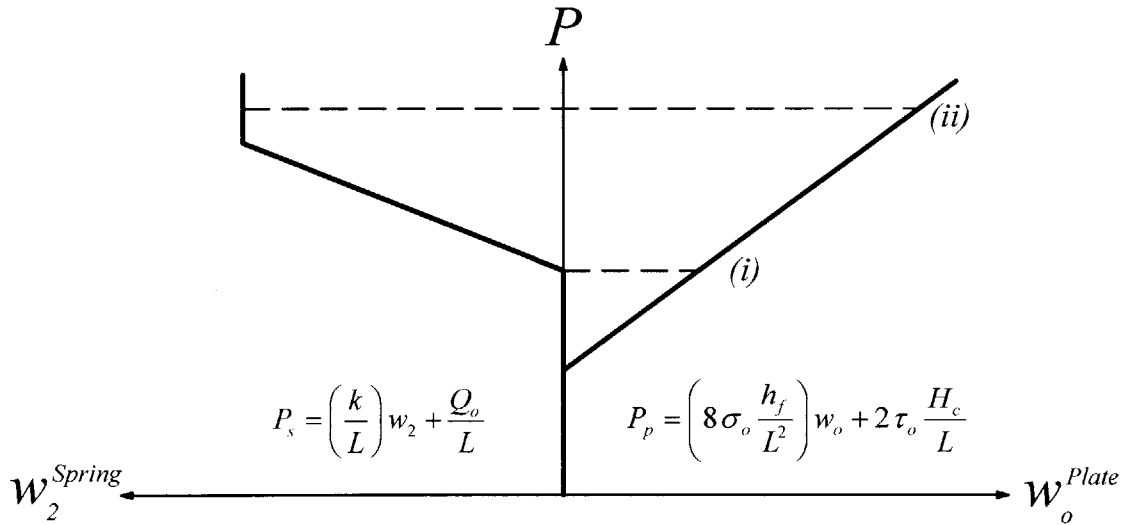


Figure 32 – Load-Displacement for Hardening Crushable Connections, Case 1.

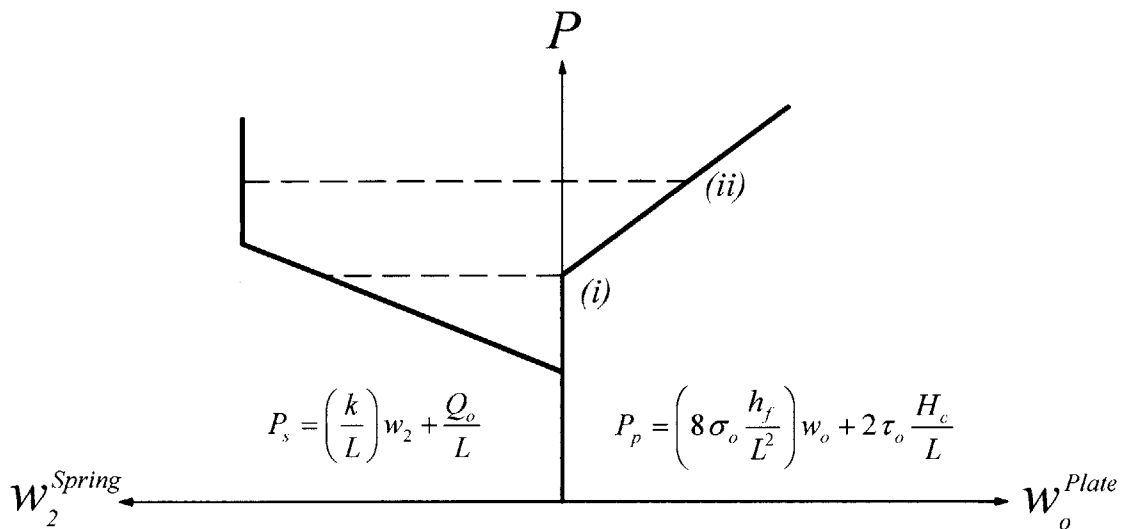


Figure 33 – Load-Displacement for Hardening Crushable Connections, Case 2.

For **Case 2**, in which $Q_o/L < 2\tau_o H_c/L$, the combined response of the sandwich plate and crushable connection is very similar to that described above. However, as shown in figure 33 the connections are the first to deform until reaching point (i) at which time the load exceeds $2\tau_o H_c/L$. Continued deformation will be experienced by both the sandwich plate and the crushable connections until the connection reaches locking at point (ii), here, the loading is transferred entirely to the sandwich plate which continues to deform until fracture.

In both cases the presence of the crushable connections will delay the onset of fracture by reducing the deformation of the sandwich plate and will increase the amount of total energy that may be absorbed by the hull.

The softening connection response, illustrated in figure 31(b), has a more interesting response when coupled with the sandwich plate. The two cases are shown in figure 34 and figure 35. For **Case 1** the sandwich plate will begin to deform initially until such point as the load overcomes the initial rigidity of the crushable connections, point (i). Since the

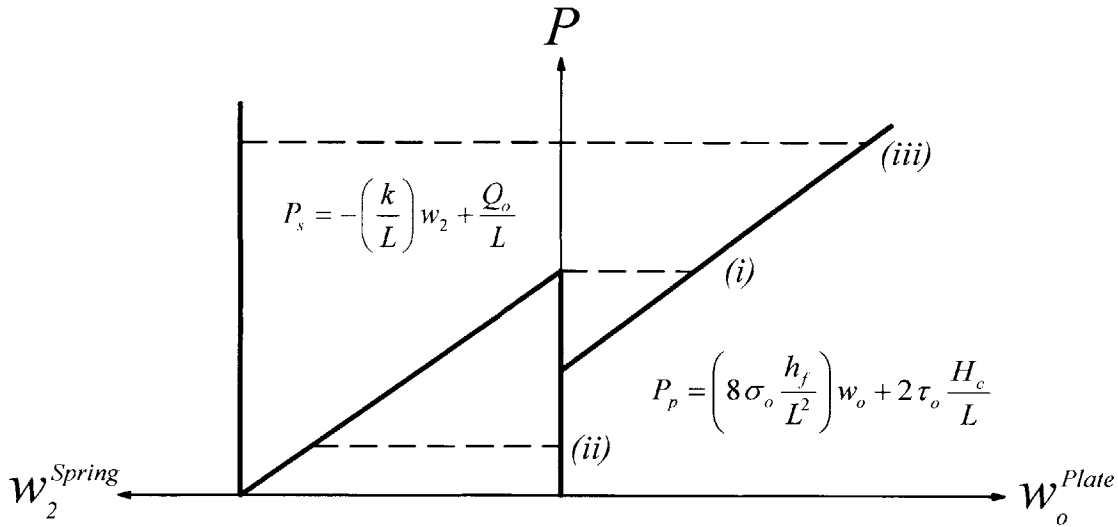


Figure 34 – Load-Displacement for Softening Crushable Connections, Case1.

connection does not harden under increasing loads, it will fail catastrophically, point (ii), until it is completely crushed, at which point the connection will lock and its load carrying capacity will be infinite for this idealized model. Further increasing the load will cause the sandwich plate to continue to deform beyond point (i) until failure occurs. In this scenario the presence of the softening crushable connection reduces the energy dissipated and under the quasi-static assumption the deformation of the sandwich plate would be carried out essentially uninterrupted by the crushing of the connections. Furthermore, the presence of the crushable connections will also help to spread the load absorption out over multiple sections through membrane stretching.

The second case, shown in figure 35, produces much the same results; that is, the crushable connection will fail without delaying the deformation of the sandwich plate. After the initial rigidity of the connections is overcome at point (i) the connections dynamically collapse and the load is then carried by the sandwich plate until yielding begins at point (ii).

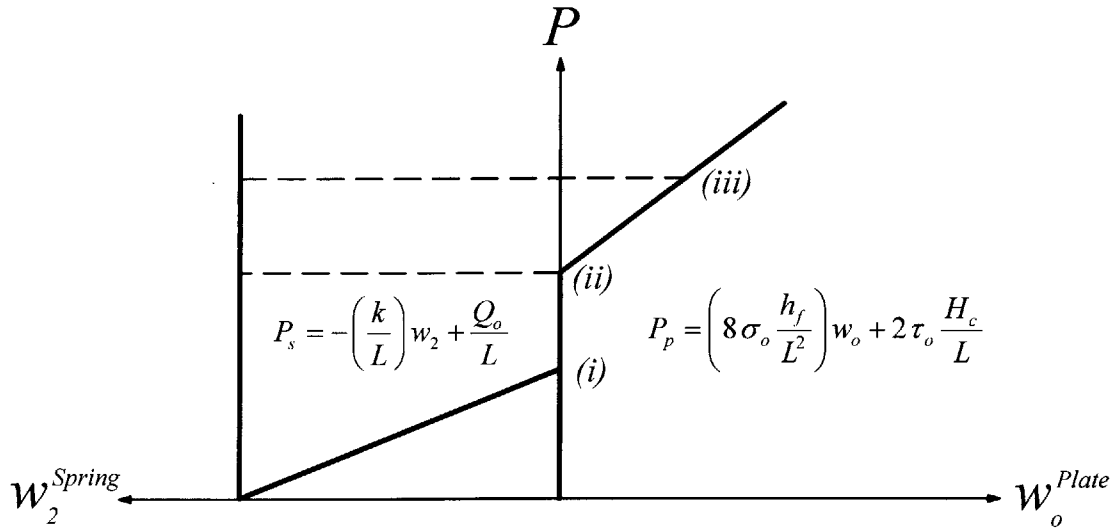


Figure 35 – Load-Displacement for Softening Crushable Connections, Case 2.

The sandwich plate then continues to deform until failure.

The third pairing is a combination of the sandwich plate and the analytical solution proposed by Wierzbicki and Abramowicz [3] for a circular cross-section as shown in equation (4.4.1)(c). Due to its hardening behavior as it advances asymptotically toward locking, this system behaves in a similar fashion to the linearly hardening model. From

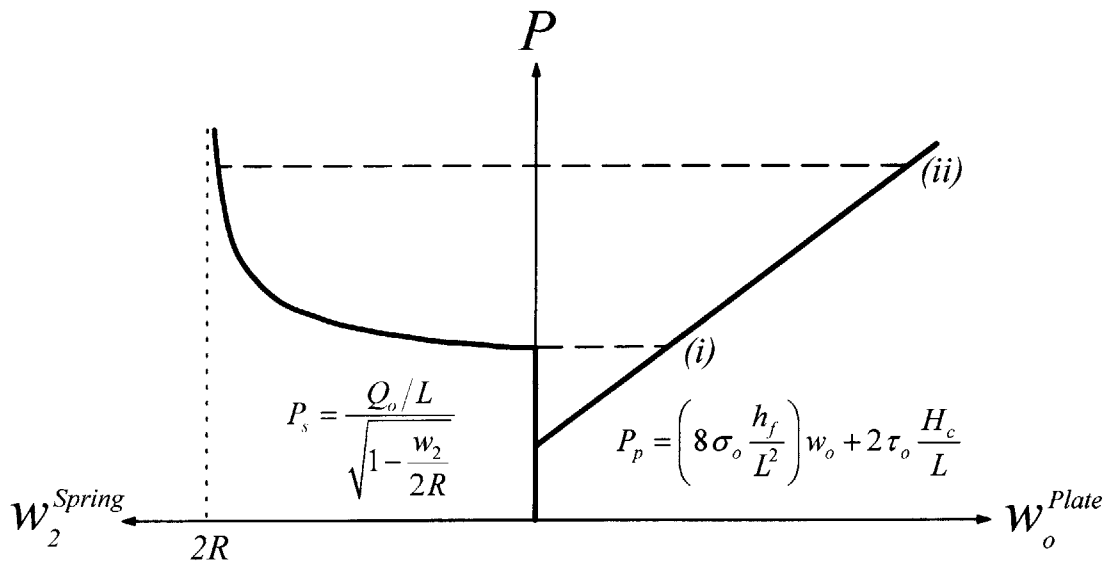


Figure 36 – Load-Displacement for Circular Section Crushing, Case 1.

figure 36 it can be seen that the sandwich plate will initially deform until point (i) where the load increases above the initial rigidity of the crushable connection. At this load the crushable support will begin to deform along with the sandwich plate, reducing the energy absorbed by the plate and helping to carry the load. By further increasing the load P the maximum deflection of the crushable connection w_2 will approach $2R$ the total available crushable height of the support. Once the support has fully crushed and locked, its load carrying capacity becomes infinite (point (ii)) and the sandwich plate continues to deform under the entire load until fracture occurs.

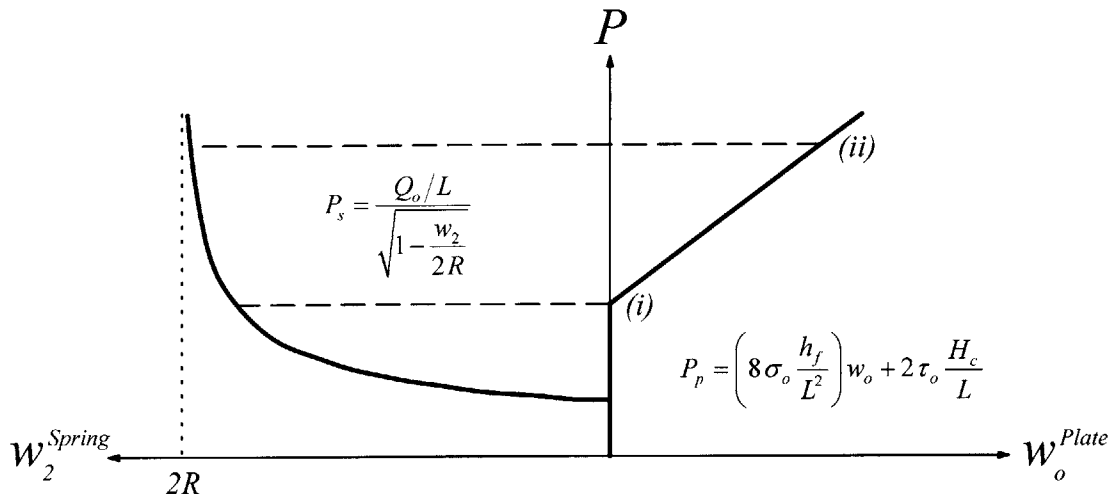


Figure 37 – Load-Displacement for Circular Section Crushing, Case 2.

The load-displacement relationship in figure 37 shows the second case where the crushable connections deform prior to the sandwich plate. The connections will begin to yield when $P = Q_o/L$ and will continue to deform until point (i). Once the initial rigidity of the sandwich plate is exceeded, the panel will begin to deform. Both the crushable supports and the sandwich plate will deform together until the crushable supports lock. Once the supports no longer deform, at approximately point (ii) the sandwich plate itself absorbs the energy of the loading P until it reaches the point of fracture. This loading configuration, as shown in figure 37 offers the same benefits that the linear hardening load-displacement function provided. By deforming along with the sandwich plate, the load experienced by the panel and consequently the deformation experienced by the panel would be reduced. This reduction in deformation would allow such a structure to absorb more energy and withstand higher loadings prior to the onset of fracture.

The final practical loading curve examined was for the crushing of a diamond shaped cross-section. This shape was identified in Chapter 3 and its combination with a sandwich panel will yield very similar results as for that of a linear softening model. With reference to figure 38, for a **Case 1** configuration the initial rigidity of the sandwich panel is overcome first and the panel begins to deform plastically. Once the load has increased above Q_o/L , at point (i), the connections begin to crush. Since the diamond shaped connections have a softening crushing reaction the supports will deform dynamically and catastrophically until locking is reached. At this point, as with all of the previously described configurations, the

load carrying capacity of the supports is assumed to be infinite and the load is instantaneously transferred entirely to the sandwich plate at point (i) and continues to be carried by the sandwich plate until failure.

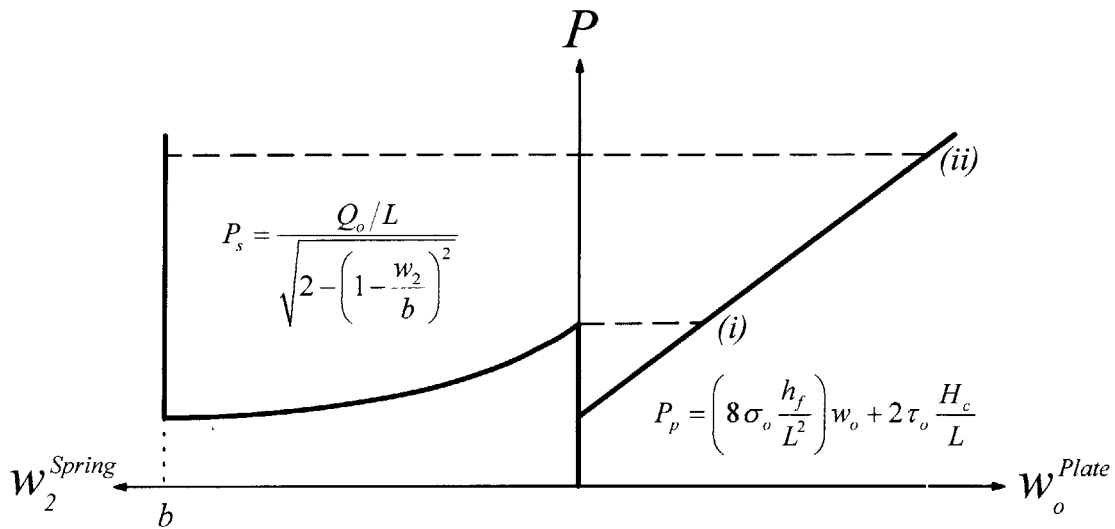


Figure 38 – Load-Displacement for Diamond Section Crushing, Case 1.

The second case for a hollow diamond cross-section is a configuration in which the crushable connections begin to yield prior to the load overcoming the sandwich plate’s initial rigidity. The load displacement diagram for this scenario is shown in figure 39. From the figure, it can be seen that at point (i) the supports will begin to collapse. Once again, due to

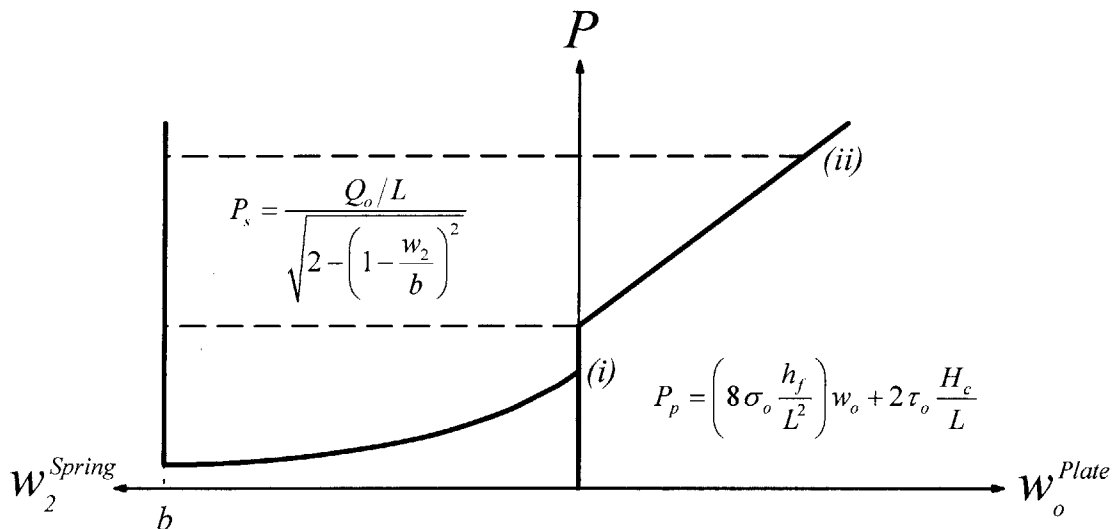


Figure 39 – Load-Displacement for Diamond Section Crushing, Case 2.

the softening response of the crushable connections a dynamic deformation will occur in which the connections crush to locking. As the load continues to increase the sandwich plate will begin to deform and will carry the full load until such time as the plate fails.

4.5 Numerical Example

A numerical example was also solved to further quantify the relationship between the crushing of the supports and the deformation of the sandwich panel. Similar to the previous section, the sandwich beam model will be used, not only for the simplicity of the mathematics but also due to the availability of a core shear stress value from Xue and Hutchinson [6]. Using the notation introduced in figure 23 and the following values from Xue and Hutchinson for a sandwich panel made of 304 Stainless Steel:

$$\sigma_o = 205 \text{ MPa} \quad \tau_o^{Average} = 2.22 \text{ MPa} \quad \frac{H_c}{L} = 0.1 \quad \frac{h_f}{H_c} = 0.08$$

where $\tau_o^{Average}$ is the average of the lower and upper bound shear values previously reported from figure 25. Substituting these values into equation (4.2.10) produces an equation for the deflection of a sandwich panel as a function of the dimensionless displacement w_o/L :

$$p_p = (13.12) \frac{w_o}{L} + (0.44) \text{ [MPa]}. \quad (4.5.1)$$

For the crushable support the above stated quantities can be substituted into equation (4.2.11). If it is assumed that the connections have a response similar to that shown in equation (4.4.1)(c) for a circular cross-section and a height equal to the thickness of the core ($2R = H_c$) the following relation can be found:

$$p_s = \frac{Q_o}{L} \frac{1}{\sqrt{1 - 10 \left(\frac{w_2}{L} \right)}}. \quad (4.5.2)$$

As in Section 4.4, the ratio between the initial rigidity of the sandwich panel and the initial rigidity of the crushable supports differentiates the varying design configurations. To examine a broad range these two initial values can be parameterized such that the initial rigidity of the crushable support is some constant multiple C of the initial rigidity of the sandwich plate:

$$\frac{Q_o}{L} = C(0.44) \text{ [MPa]}. \quad (4.5.3)$$

Substituting equation (4.5.3) into equation (4.5.2) yields:

$$p_s = \frac{C(0.44)}{\sqrt{1 - 10 \left(\frac{w_2}{L} \right)}} \text{ [MPa]}. \quad (4.5.4)$$

Making use of the same graphical representation used in the previous section, figure 40 shows a parametric depiction of the relationship between the crushing of the supports and the deformation of the sandwich plate under quasi-static loading. The plot was created by varying C and plotting equation (4.5.1) and equation (4.5.4) against their respective non-dimensionalized displacements.

Parametric Analysis of Varying Initial Rigidity of Crushable Connections

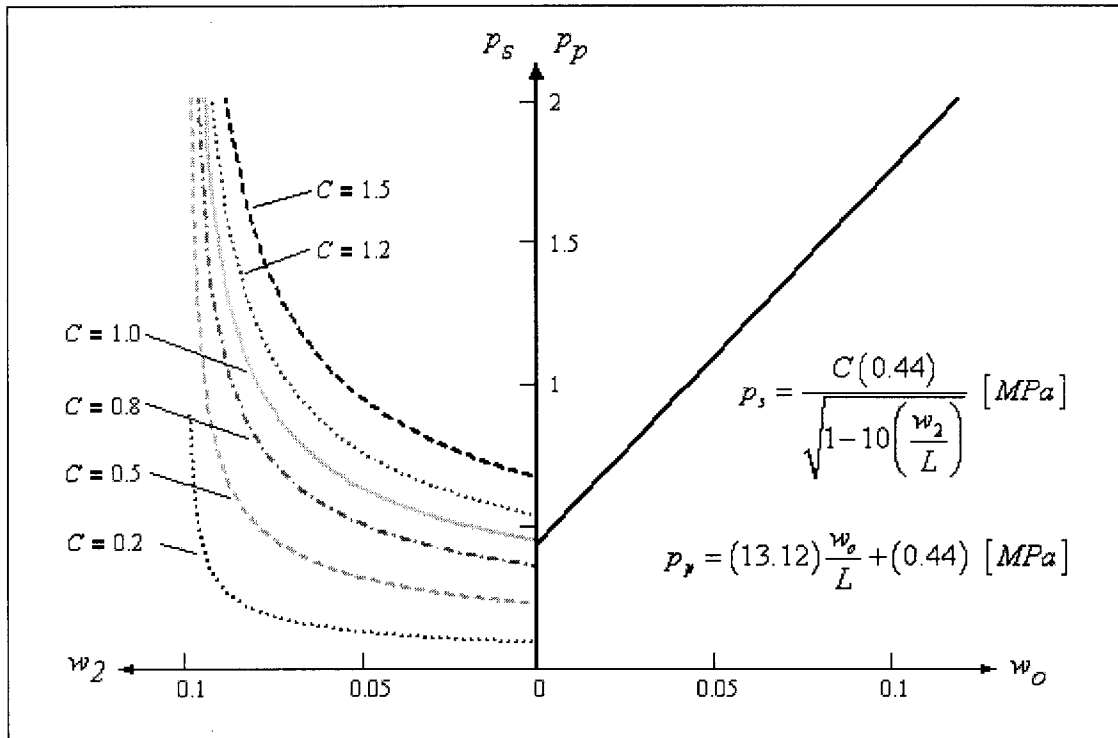


Figure 40 – Parametric Analysis of Varying Ratio of Initial Rigidity of Crushable Connections to Initial Rigidity of Sandwich Panel

Figure 40 demonstrates the same behavior as was previously discussed for crushable supports with a hardening response characteristic. The plot illustrates that by increasing the value of Q_0/L not only is the interaction between the supports and the sandwich panel changed but that the supports stiffen, providing more resistance to crushing. Balancing the locking point, the ratios of initial rigidity and the rate of increasing or decreasing stiffness will all be important variables to consider in the implementation of such a system.

4.6 Summary of Relevance to Hull Failure

Although the preceding discussion identified a variety of methods in which the crushable supports can interact with the sandwich panel during a loading event, the most important aspect, with regards to this project, is the increase in energy dissipation and delaying of fracture that will occur. The addition of crushable supports increases the total energy that the system is capable of absorbing prior to failure. Figure 41 shows a load-displacement curve for a sandwich panel continuing until the point of failure defined by a

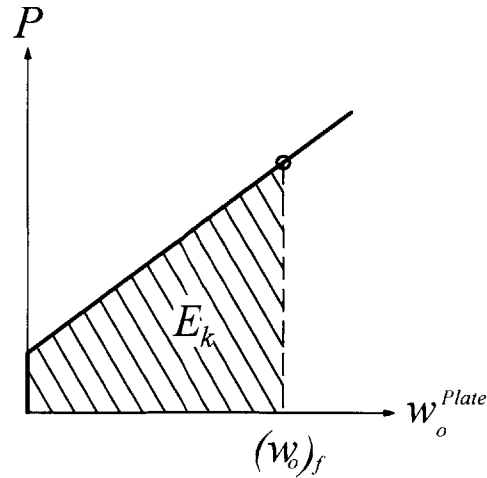


Figure 41 – Energy Dissipation for a Rigidly Supported Sandwich Panel.

displacement of $(w_o)_f$. The energy dissipated by the sandwich plate E_k during this event is equivalent to the area under the curve. If a crushable support is now introduced and designed in such a way that it deforms along with sandwich panel, as we have previously assumed, then the total energy dissipated is going to increase. From figure 42 it is plain to see that the total energy absorbed by such a system would be the sum of E_1 and E_2 . Due to the addition of the crushable supports and the increased energy absorption that they provide, the sandwich panel will deform less for a given loading P and thus fracture will be delayed.

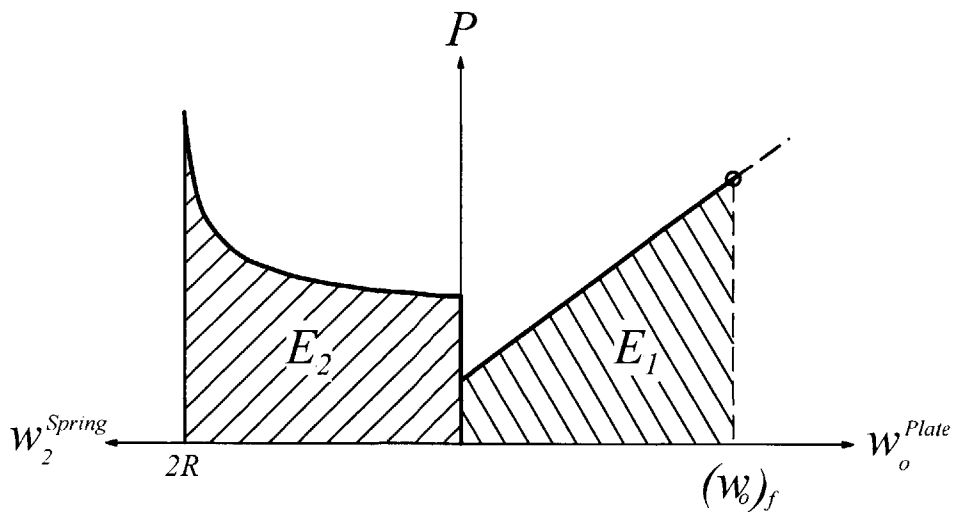


Figure 42 – Combined Energy Dissipation for a Sandwich Panel on Crushable Supports.

Chapter 5

CONCLUSIONS AND RECOMMENDATIONS

5.1 Conclusions

Analytical investigations have been carried out into two main areas: the crushing of a sandwich panel on a rigid base; and the deformation of a sandwich panel on crushable supports. The plane stress crushing of a sandwich panel on a rigid base was solved for both a knife edge indentation and a flat punch indentation. The knife edge indenter can be seen to simulate the crushing of a double hull due to a loading which may be caused by the pinnacle of a submerged rock or by collision with another ship. In order to simulate the shock front of a close proximity blast the flat punch indenter was used; however, it could also quite capably represent a collision with a blunt object. In both cases, very compact solutions, summarized at the end of Chapter 2, were found for both the deformation shape normalized by the maximum displacement as well as for the particular load-displacement curve for such an incident. These analytical solutions can provide quick and effective means for validating finite-element solutions as well as giving initial engineering approximations.

The addition of crushable connections to support double-hull or sandwich panel construction was analytically quantified for a single panel section. Two mathematical models were solved: a two-dimensional, plane stress beam/strip model; and a three-dimensional, fully supported plate model. In solving the beam/strip model representation independent linear load-displacement functions were found for both the sandwich panel and the crushable supports. The analytical solution for the sandwich panel was contrasted with previously published numerical solutions and was shown to closely reproduce the load-displacement behavior.

The three-dimensional model was solved using a plastic hinge-line approximation for the deflection profile and assuming identical crushable supports fixed around its periphery. With simplifying assumptions, the load-displacement behavior of a plastically deforming, three-dimensional plate, experiencing a constant distributed load was found. The resulting function, similar to the beam/strip model, showed a linear relationship.

Recognizing that since both the beam/strip model and the plate model deformed according to a linear relationship, the much simpler beam model could be examined for its interaction with the crushable supports without any loss of generality. A solution using the plate model would interact in a very similar manner although mathematically the coefficients of the linear load-displacement function would be more complicated. A graphical representation of the interaction between the sandwich panel and the crushable supports under quasi-static loading allowed for a thorough understanding of the design choices that will become important in such a problem. The crushable supports that demonstrated a hardening characteristic were shown to delay fracture by reducing the deflection of the sandwich panel for a given load. Furthermore, they increased the overall energy absorption

of the system allowing a ship's hull to withstand higher energy events prior to failure. Similarly, the crushable supports which displayed a rigid-linear softening behavior under loading would also increase the total energy dissipated by the ship's hull, although they are not likely to delay fracture as much as similar supports which demonstrate a hardening response.

From these simplified analytical investigations, solutions which explain and quantify the first order behavior of sandwich panels on crushable connections were found. These solutions will help to validate numerical modeling which is already being carried out in the Impact and Crashworthiness Lab. Furthermore, the benefits of such a system were clearly shown through the interaction of the sandwich panel with the crushable supports.

5.2 Recommendations

The analytical investigation of such a problem is very simply the first step in researching a new application. Although further refinement of the analytical model is not likely to produce significant gains in understanding, creation and exploration of numerical models will. The interaction between the crushable connections and the sandwich panel itself is seen to be an interesting area of further inquiry. There is an exceptionally large range of plausible support shapes and responses as well as myriad ways in which the support's reaction can vary in comparison to the sandwich panel's reaction. In parallel to the theoretical design of this system the physical design will also present many challenges in way of costs and producibility that must be thoroughly researched and investigated.

Bibliography

- [1] Wierzbicki, T. and Suh, M.S. "Indentation of Tubes under Combined Loading." *International Journal of Mechanical Science*. 1988; Vol. 30, No. 3/4: pp.229-248.
- [2] Wierzbicki, T., de Lacruz Alvarez, A., and Hoo Fatt, M.S. "Impact and Energy Absorption of Sandwich Plates with Crushable Core." *Impact, Waves and Fracture*. 1995; AMD-205, pp.391-411. (ASME)
- [3] Wierzbicki, T. and Abramowicz, W. The Mechanics of Deep Plastic Collapse of Thin-Walled Structures. In: Wierzbicki, T., Jones, N. editors. *Structural Failure*. John Wiley & Sons; 1989. 281-329.
- [4] Abramowicz, W. Crush Resistance of "T", "Y" and "X" Sections. Joint MIT – Industry Project on Tanker Safety. January 1994.
- [5] Wierzbicki, T. and Abramowicz, W. Development of a Superelement for Laterally Crushed Components of a Car Body. Impact and Crashworthiness Lab, May 2001.
- [6] Xue, Z. and Hutchinson, J.W. Constitutive Model for Metallic Sandwich Cores. Division of Engineering and Applied Sciences, Harvard University. 2004.
- [7] Wiernicki, C.J. Damage Assessment of Ship Plating Subjected to Hydrodynamic Impact Loading. Cambridge, MA: Massachusetts Institute of Technology; Ocean Engineering Thesis, 1985. 147 p. MIT Barker Library - Microforms.

- [8] Hoo Fatt, M.S. and Wierzbicki, T. "Damage of Plastic Cylinders under Localized Pressure Loading." *International Journal of Mechanical Science*. 1991; Vol. 33, No. 12: pp.999-1016.
- [9] Wierzbicki, T. and Doyoyo, M. "Determination of the Local Stress-Strain Response of Foams." *Journal of Applied Mechanics*. 2003 March; Vol. 70, pp. 204-211.
- [10] Rodd, J.L. and McCampbell, S. Double Hull Tanker Grounding Experiments. The Advanced (Unidirectional) Double-Hull Technical Symposium; 1994 October 25-26; Gaithersburg, Maryland. Sponsored by the United States Navy and the Maritime Administration.
- [11] Rodd, J.L., Phillips, M.P. and Anderson, E.D. Stranding Experiments on Double Hull Tanker Structures. The Advanced (Unidirectional) Double-Hull Technical Symposium. Sponsored by the United States Navy and the Maritime Administration. 1994 October 25-26; Gaithersburg, Maryland.
- [12] Vinson, Jack R. *The Behavior of Sandwich Structures of Isotropic and Composite Materials*. Lancaster, PA: Technomic Publishing Company; 1999. 378 p.
- [13] Frostig, Y. and Baruch, M. "Bending of Sandwich Beams with Transversely Flexible Core." *AIAA Journal*. 1990 March; Vol. 28, No. 3: pp.523-531.
- [14] Frostig, Y., Baruch, M., Vilnay, O., and Sheinman, I. "High-Order Theory for Sandwich-Beam Behavior with Transversely Flexible Core." *Journal of Engineering Mechanics*. 1992 May; Vol. 118, No. 5: pp.1026-1043.
- [15] Frostig, Y. and Baruch, M. "Localized Load Effects in High-Order Bending of Sandwich Panels with Flexible Core." *Journal of Engineering Mechanics*. 1996 November; Vol. 122, No. 11: pp.1069-1076.